




ADP release can explain spatially-dependent kinesin binding times

Trini Nguyen^{1†}, Babu Janakaloti Narayanareddy ^{2†}, Steven P. Gross ^{1,2,3,4*}, and Christopher E. Miles ^{1,5,6*}

¹Center for Complex Biological Systems

²Department of Developmental and Cell Biology

³Department of Physics and Astronomy

⁴Department of Biomedical Engineering

⁵Department of Mathematics

⁶Center for Multiscale Cell Fate, University of California, Irvine, Irvine, CA 92697

November 7, 2023

[†]Co-first authors

*Corresponding Authors: Steven P. Gross, 2222 Nat. Sci I, Irvine, CA 92697, Email: sgross@uci.edu; Christopher E. Miles, 340G Rowland Hall, Irvine, CA 92697, E-mail: chris.miles@uci.edu

Classification: Biophysics and Computational Biology

Keywords: intracellular transport, biophysics, motor proteins, ADP release, protein-protein interactions, simulation-based inference

Abstract

The self-organization of cells relies on the profound complexity of protein-protein interactions. Challenges in directly observing these events have hindered progress toward understanding their diverse behaviors. One notable example is the interaction between molecular motors and cytoskeletal systems that combine to perform a variety of cellular functions. In this work, we leverage theory and experiments to identify and quantify the rate-limiting mechanism of the initial association between a cargo-bound kinesin motor and a microtubule track. Recent advances in optical tweezers provide binding times for several lengths of kinesin motors trapped at varying distances from a microtubule, empowering the investigation of competing models. We first explore a diffusion-limited model of binding. Through Brownian dynamics simulations and simulation-based inference, we find this simple diffusion model fails to explain the experimental binding times, but an extended model that accounts for the ADP state of the molecular motor agrees closely with the data, even under the scrutiny of penalizing for additional model complexity. We provide quantification of both kinetic rates and biophysical parameters underlying the proposed binding process. Our model suggests that most but not every motor binding event is limited by their ADP state. Lastly, we predict how these association rates can be modulated in distinct ways through variation of environmental concentrations and spatial distances.

Significance Statement

Cytoskeletal-motor assemblies self-organize to achieve cellular functions ranging from delivering intracellular cargoes to generating forces in mitosis. Advancements in single-molecule experiments have revealed immense detail about motor detachment and stepping, but relatively little regarding the attachment process. With newly available spatially parameterized motor binding times from an optical trap, the evaluation of mechanistic models for binding becomes possible. We find that a model limited by both diffusive search and ADP-release best explains the data. The coupled chemo-mechanical nature of this interaction is more malleable than either separately, possibly explaining the rich diversity and regulation observed in cells. More broadly, our study provides a timely vignette on leveraging computations with experiments to understand how geometry and other complexities shape protein-protein interactions.

Introduction

Life depends on an immensely diverse and complex array of protein-protein interactions [1]. These interactions are richly regulated in both space and time (e.g., via post-translational modifications, fluctuating concentrations [2]) to modulate affinities, promiscuities, and sensitivities [3]. Understanding how these interactions are parameterized by both chemical and physical factors is broadly limited due to challenges in observing interaction events directly [4]. While predicting interactions from molecular structures (e.g., from molecular dynamics simulations) is an invaluable approach, these investigations still suffer from the same observational limitation in their validation [5].

One variety of such interactions of diffuse importance across cellular function are those between molecular motors and cytoskeletal filaments. Cytoskeletal motors, specifically kinesin-microtubule assemblies, self-organize to perform a zoo of cellular behaviors, including the delivery of cargoes in intracellular transport [6], generation of forces to guide genetic material in mitosis [7, 8], and guiding of axonal growth [9]. Each of these wildly different behaviors is fundamentally achieved through molecular motors binding, stepping, and unbinding from cytoskeletal filaments [10]. Over the last several decades, advancements in single-molecule experiments have revealed extensive details about the latter two components [11–13]. Stepping and unbinding are, in some sense, *downstream* of binding, suggesting clear merit in understanding the details underlying the process.

Pursuits toward understanding motor-cytoskeleton binding have been clouded by complications in disentangling the measurements from convolving factors. That is, one must specify exactly the notion of binding that is being measured. To do so, consider the full process of self-assembly. Initially, a freely diffusing motor associates with a cargo, the motor-cargo complex then diffuses to close proximity to a cytoskeletal filament, and then the first motor binds to this cytoskeletal filament. After this initial binding, other motors associated with the cargo attach to the filament and go through cycles of reattachment. Due to the challenges in disentangling these steps, there is

65 enormous variety in the reported ranges for binding rates. While landing rate assays [14] provide direct measure-
66 ments of motor-cargo association rates, these do not inform motor-cytoskeletal rates. With the exception of [15],
67 very little data of direct measurements of motor-microtubule binding events exists, but this study corresponds to
68 the reattachment of a secondary motor that is kept in close proximity to the filament by another. Effective binding
69 on the timescale of seconds [16, 17] to tenths of a second [18] have been reported from indirect measurements
70 and utilized heavily in other modeling works [19–22] to understand collective motor behavior. However, these ef-
71 fective rates neglect geometric factors (such as organization on the cargo) that are known to crucially dictate the
72 binding rate [23–26]. A mechanistic, biophysical model of the binding process is therefore necessary to reconcile
73 the various experimental observations and modeling efforts.

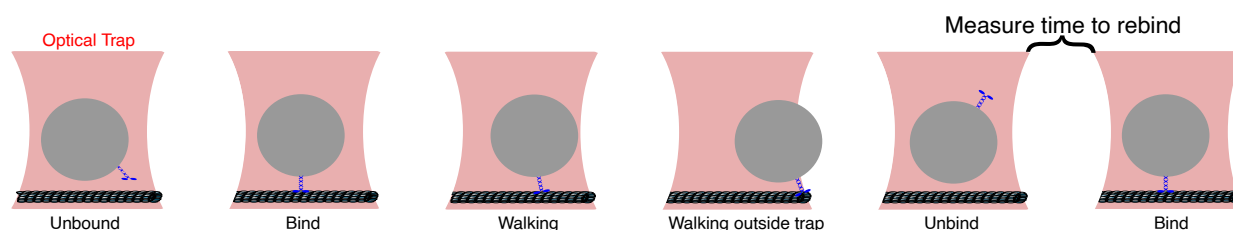


Figure 1: Experimental setup. An optical trap (pink) controls the average z -position of a polystyrene microbead cargo. When the cargo-motor ensemble binds to the microtubule and begins to walk on it, a position-sensitive diode (PSD) senses the displacement of the bead. As the motor walks farther from the center of the trap, the force on the cargo (and consequently the motor) grows, eventually leading to unbinding from the microtubule and resetting of the setup. The PSD measurements provide the timing between unbinding to rebinding, the binding process modeled throughout the remainder of the work.

74 Here, we use a combined experimental and computational approach to explore different possible biophysical
75 models of how the motor-microtubule binding process occurs. The investigation is based on the initial associ-
76 ation time between a cargo-bound kinesin and microtubule from recent optical trap measurements (**Fig. 1**) on
77 a variety of motor lengths and trapped distances away from the microtubule. The span of setups allows explo-
78 ration and validation of models otherwise impossible with a single dataset. We first investigate the null model of
79 a diffusion-limited search performed by the motor head. Through Brownian dynamics simulations coupled with
80 simulation-based inference, we find that this model fails to capture a delay in binding at close distances. We
81 find reconciliation with the data after the addition of an ADP-release requirement prior to binding to the model,
82 motivated by known mechano-chemistry of motors. Through approximate Bayesian computation techniques, we
83 quantify underlying rates and biophysical parameters governing this process and predict that most motor binding
84 events are limited by tubulin-stimulated ADP release. Lastly, we provide predictions on how this process can be
85 modulated distinctly by varying environmental concentrations or spatial distance, highlighting the complexity and
86 regulatability of this interaction. Altogether, our study provides a new state-of-the-art mechanistic understanding
87 of the motor-cytoskeletal binding process, a crucial ingredient in understanding the self-organization of motor-
88 cytoskeletal assemblies used in cellular function. More broadly, our work illustrates how complexities arising from
89 spatial and chemo-mechanical factors that shape protein-protein interactions may be understood through the
90 combined efforts of theory and experiments.

91 Results

92 Diffusion-limited binding does not capture the qualitative behavior of experimental data.

93 To investigate the biophysical mechanisms of the first association between a cargo-bound motor and a micro-
94 tubule, we compare binding time data of three kinesin lengths (33, 45, and 60 nm) attached to a polystyrene
95 bead that is laser-trapped at several distances away (0, 20, 40, and 60 nm) from a microtubule. Concentrations
96 of motors in solution are diluted such that at most one motor is on each bead. Throughout the remainder of the
97 work, we consider the binding time to be that between the unbinding reset event and the next time of detectable
98 direction of the bead, as schematically shown in **Fig. 1**. See Materials and Methods for further details on the

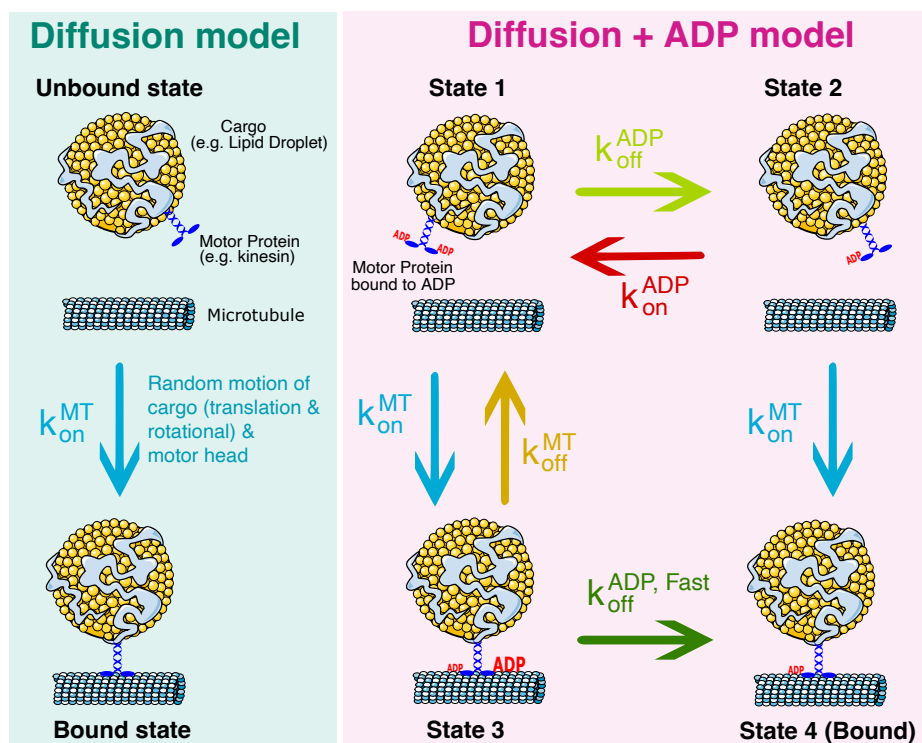


Figure 2: Schematic of models. Left: State diagram of the simple diffusion model of kinesin-microtubule binding. Through random motion of the cargo and motor head, binding time is determined by the stochastic search process of the motor reacting when in close proximity to the microtubule. Right: Model of binding process that considers ADP release. We consider a cargo-motor ensemble that is in State 1, unbound from the microtubule and bound to ADP on both motor heads. From here, the motor can release ADP from one of its heads, transitioning to State 2, or bind weakly to the microtubule in State 3. To bind strongly to the microtubule and transition to State 4, the motor must meet two requirements: ADP is released from one of its motor heads and it must be within a binding distance to the microtubule. We consider two types of ADP release: a non-tubulin stimulated rate (k_{off}^{ADP}), and a faster tubulin-stimulated rate ($k_{off}^{ADP, Fast}$).

99 experimental setup. The resulting binding times can be seen in **Fig. 3ABC** (black). Times are on the order of
 100 seconds, which is in line with other measurements of binding as discussed in the Introduction. Intuitively, as the
 101 cargo is moved away from the microtubule track, binding times increase. The most straightforward explanation
 102 for this is a "random search" mechanism rate-limiting the binding, schematically shown in **Fig. 2** as the "diffusion
 103 model". That is, the "null" model for binding, as assumed elsewhere [10], is that the motor head undergoes
 104 random motion until it reaches close proximity to the microtubule track and then binds with some reactivity.

105 To investigate whether such a diffusion-binding model can explain the binding time across experimentally
 106 observed conditions, we developed a Brownian dynamics simulation of the proposed model. The stochastic
 107 model includes the random motion of the cargo, both translation and rotational, and the diffusive search of a
 108 motor head attached via a tether to this cargo. The tether is assumed to be of the known length of each motor
 109 and exerts a Hookean force when extended beyond this length. The initial configuration of the motor head is
 110 assumed to be downward, based on the fast timescale of resetting in the optical trap (tenths of a second). When
 111 the motor head enters a specified distance of the microtubule due to random motion, the binding reaction occurs
 112 at an unknown, microscopic rate. Additional model details and discussion of assumptions can be found in the
 113 Materials and Methods. Ultimately this leads to two unknown parameters: the diffusivity of the motor head, and
 114 the microscopic reactivity.

115 Through a suite of simulation-based inference techniques [27–29] (further details in Methods and Materials),
 116 we obtain fits to the diffusion model over all experimental setups for the two unknown parameters: the diffusivity
 117 of the motor head, and the microscopic binding rate. The resulting fits can be seen in **Fig. 3ABC** (green) for the

118 mean time to bind for the three motor lengths and various distances. There appears to be reasonable qualitative
 119 agreement with the experiments, where increasing distances increases binding time. The corresponding param-
 120 eter fits can be found in **Table 1**. While the diffusivity of the motor head is challenging to quantify [30], our fitted
 121 value on the order of 1000-10000 nm²/s is within ranges considered for kinesin elsewhere [31]. Upon further
 122 scrutiny, the mean binding times shown in **Fig. 3ABC**, especially at close distance display a distinct qualitative
 123 disagreement between the diffusion model and experimental measurements. In the diffusion model, as the cargo
 124 is trapped closer, the motor is effectively instantly able to bind. However, experimental values show a plateau of
 125 times around 1 second, even for close distances. This plateau points to the binding process being a multistep
 126 process.

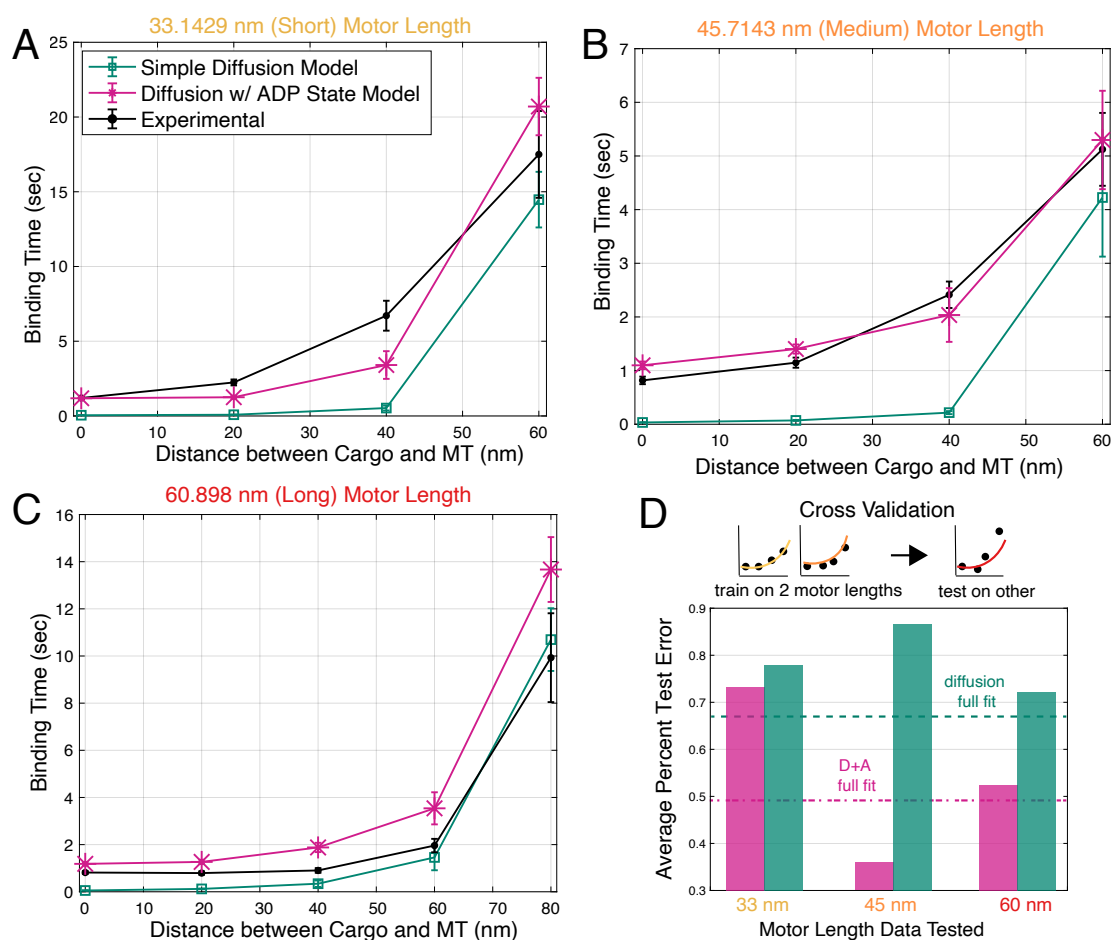


Figure 3: Model fits and cross-validation. ADP-release model captures qualitative behavior in experimental data, while the simple diffusion model cannot. *In vitro* optical trap experiments were used to measure mean binding times (black) for three motor lengths: 33 nm **A**, 45 nm **B**, and 60 nm **C**. The horizontal axis shows average distances between the cargo and microtubule (MT), which were varied for each experiment. Two binding models (simple diffusion only in blue and ADP-release in red) were simulated and fitted to the experimental data. $n = 100$ for simulated data varied for experimental data. Data are presented as mean \pm SEM. **D**: Cross-validation was performed to determine the predictive power of each model. For three rounds, data was trained on two motor lengths, and tested on the third.

127 **A chemo-mechanical ADP-release model of binding better explains observed times.**

128 With the observation that a simple diffusion model does not produce a delay in binding at close distances seen
 129 in experimental measurements, we sought a model that may explain this phenomenon. For a possible explana-

tion, we turn to the rich mechanochemistry of the kinesin motor. It is known that the nucleotide state of each motor head crucially determines its strong or weak affinity to the microtubule [32–34] and through cycles of this nucleotide state (ATP, ADP, released), processive stepping is achieved [35]. We posit that this nucleotide-based regulation of "binding" extends beyond that of processive stepping, and even the preliminary attachment between the cargo-motor ensemble and the microtubule. That is, we posit that the experimentally observed binding times correspond to a strong binding event, and therefore the underlying nucleotide state of the motor heads, plays a significant role in arriving at this state.

To investigate whether a model including nucleotide state may better explain the experimentally observed times, we extend the model to account for 4 possible states, as shown in **Fig. 2**. In this model, the motor-cargo ensemble begins in State 1 with both motor heads in an ADP state, undergoing the same random motion as the diffusion model. From here, the ensemble can enter one of two states: State 2, where ADP is released from either motor head, or State 3, when the ensemble diffuses close to the microtubule and weakly binds to it. From either of these states, the ensemble can then strongly bind to the microtubule either through diffusion (from State 2), or the ADP molecule is released (from State 3). We consider two types of ADP release, a fast tubulin-stimulated release and a slow non-tubulin-stimulated release [36–41]. We consider ADP release as a requirement for strong binding based on the neck-linker model for stepping where an ADP-bound head has a low affinity for the microtubule, then this trailing head moves forward along the microtubule bound to ADP, and when it steps down onto the microtubule, ADP is released [42]. Importantly, our description is coarse-grained to not track the heads separately, but we consider the ADP release to describe either motor head. The assumption that the ensemble begins in State 1 has two parts: we assume that if the motor detaches in an ATP-bound state, this phosphate release is fast [35], but then the corresponding ADP release is slow without tubulin [39].

Using the same simulation-based inference approaches for the diffusion model, we fit the observed binding times for all 3 motor lengths and distances simultaneously for the extended ADP-diffusion model, with 7 unknown parameters, 2 from the diffusion model, 4 reaction rates, and 1 corresponding to the strength of attachment in the weak binding state. The result of the fits can be seen in **Fig. 3ABC** in pink. The overall fit is discernibly better for the 33 nm and 45 nm motor lengths, and arguably worse for 60 nm at long distances, but notably, the model now captures the qualitative feature of a plateau of times at short distances. While only the mean binding times were used to fit, **Figs. S.2 and S.3** show close agreement in full distributions of binding times as well.

Beyond the qualitative improvement, the inherent danger in quantitatively assessing whether the ADP-release model better explains the data comes from the increased model complexity [43]. Intuitively, a model with more parameters has more flexibility to produce a better fit, and careful attention must be paid to model selection. In lieu of commonly-used information-theoretic techniques (AIC, BIC), even for simulation-based inference [44], we instead leverage the structure of our experimental observations to compare models based on their ability to explain unseen experimental circumstances. We perform a cross-validation procedure where we fit both the diffusion and ADP+diffusion models to the binding times for 2 of the 3 motor lengths, withholding one for testing on the trained models. In each validation test of withholding a motor length, the more complex model generalized better, shown in **Fig. 3D**. From this, we conclude that the ADP-diffusion model better explains the observed binding times, even under cross-validation-based scrutiny [45].

Kinetic and biophysical parameters of the ADP-binding model can be estimated.

Beyond the qualitative lesson of identifying the ADP-diffusion model as explaining the data, our fitting procedure provides rich quantitative insight into the underlying processes by estimating underlying parameters, shown in **Table 1** and **Fig. 4**. Some kinetic rates have been previously measured, and serve as support for the model, whereas others are, as far as we know, unmeasured. The values reported in **Table 1** are point estimates from a simulation-based inference optimization procedure [27]. The values that have been previously measured agree within an order of magnitude. As validation of this optimization procedure for point estimates, we also performed a separate simulation-based inference technique, sequential approximate Bayesian computation (sABC) [28] to obtain samples of an (approximate) posterior distribution shown in **Fig. 4**. The reason for this method was two-fold: for one, the agreement between the point estimates arising from the two procedures validates the approximations involved in the techniques, and the latter sABC approach produces valuable uncertainty quantification that we were unable to employ but may very well be possible using the techniques of [27]. Further details on these procedures can be found in the Materials and Methods. Somewhat surprisingly, all parameters of the model seem to be identifiable, as shown in the relatively tightly-shaped posterior distributions.

Parameter	Simple Diffusion Model	Diffusion w/ ADP State Model	Previous Literature
$k_{\text{off}}^{\text{ADP}}$ (s^{-1})	0	0.008	0.008-0.1 [36, 37, 40, 41]
$k_{\text{off}}^{\text{ADP,fast}}$ (s^{-1})	0	2.12	1.14-300 [37-41]
$k_{\text{on}}^{\text{ADP}}$ (s^{-1})	0	883.8584	425 [41]
$k_{\text{on}}^{\text{MT}}$ (s^{-1})	80.5925	70.652	
$k_{\text{off}}^{\text{MT}}$ (s^{-1})	0	0.2	0.31 [46]
D_m ($\text{nm}^2 \text{s}^{-1}$)	4459.8	1994	
κ_w (pN nm^{-1})	0	0.002	

Table 1: Fitted Parameters. D_m is the diffusion constant of the tethered motor head. κ_w is the stiffness constant of the weak bond between the motor and the microtubule when the motor is weakly bound to it. Parameters are fitted using a Bayesian optimization algorithm [27]. Some parameters were not found in previous literature.

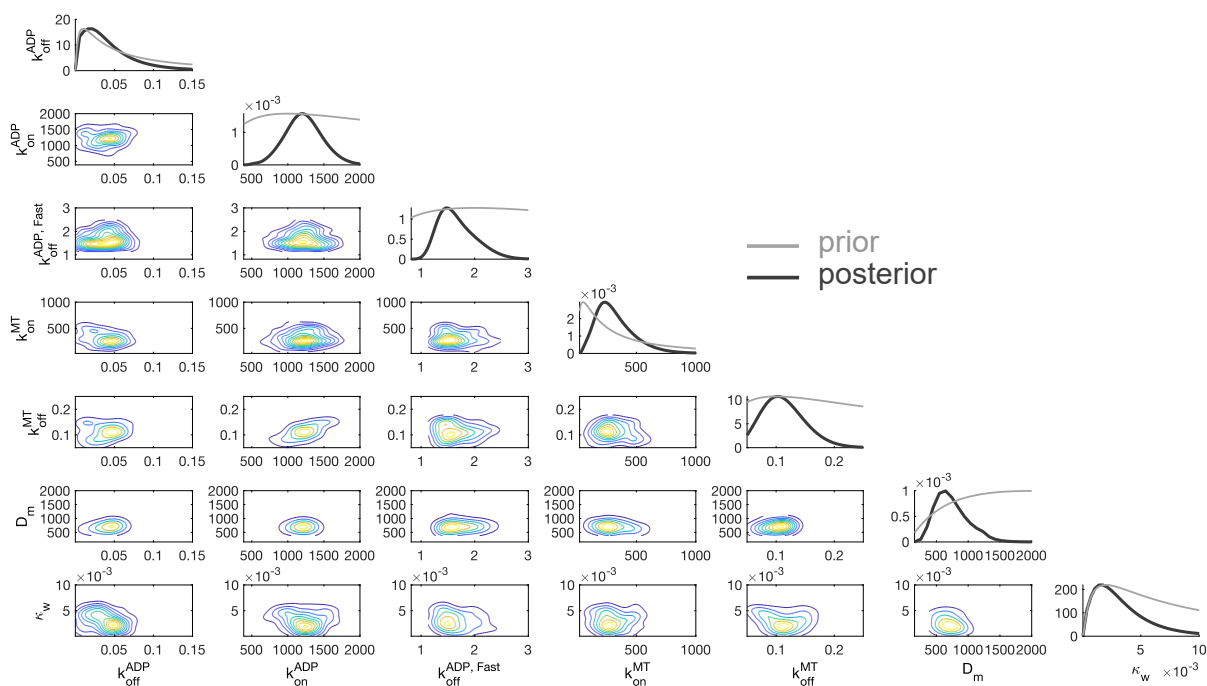


Figure 4: Estimates of microscopic parameters from fitting the ADP-diffusion model. Joint (Approximate) Posterior Distribution of ADP release Model Parameters. Black curves in the marginal densities from approximate Bayesian Computation (ABC) are the posterior distributions, and the grey curves are the priors. A kernel density estimator [47] was applied to discrete samples to form posterior estimate curves.

Most motors strongly bind via tubulin-stimulated ADP release.

These quantitative estimates of the underlying microscopic rates also provide conceptual lessons about motor binding. Referring to the model schematic in **Fig. 2**, motors are able to achieve the strong binding state either through an intermediate weak binding state (State 3) after which ADP release occurs, or directly from a diffusing state (State 2). Although we do not observe these transitions directly, their relative proportions can be deduced from the data and can be seen in **Fig. 5** for all motor lengths and distances. **Fig. 5A** shows that for all motor lengths, the frequency of the diffusion-based transition to strong binding (State 4) from diffusion (State 2) is more frequent for shorter distances. Moreover, the extent of decrease in these events is most extreme for shorter motors. These observations make sense in light of this being the diffusion-based search step. The more challenging of a search (longer distances, or shorter motor), leads to less frequent encounters. This then leaves

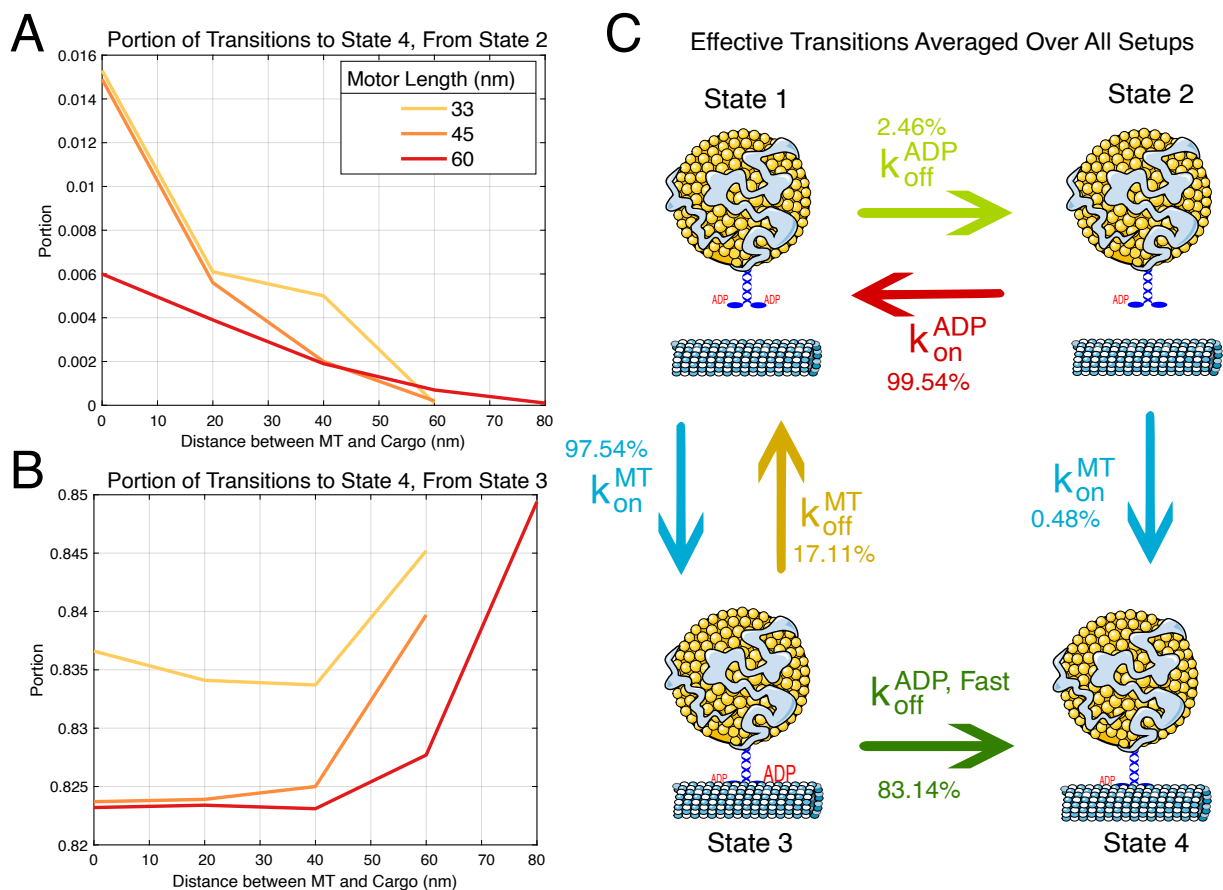


Figure 5: Cataloging typical binding events. Motors typically bind via tubulin-stimulated ADP release. Portion of transitions from States 2 (panel **A**) and 3 (panel **B**) to 4 are plotted for each motor length with respect to mean distance between the microtubule and the cargo. **C**: Mean percent of transitions that occur from each state. The mean of all events from all experimental conditions (motor length and mean spacing between cargo and microtubule) were taken. Parameters from **Table 1** were used.

192 the remaining pathway from the weak binding state, the frequency of which can be seen in **Fig. 5B**. For short
 193 distances, the frequency remains relatively constant but then increases for long distances. The overall frequency
 194 is the highest for the shortest motor and lowest for the long. These transitions intuitively complement those of
 195 the diffusive search component. While we have focused on the parameterization of these relative frequencies,
 196 the most important note is likely their overall magnitude. In **Fig. 5C**, we show our predicted percent transitions,
 197 averaged over all the experimental conditions, in which most (over 80%) of initial binding interactions arise via a
 198 preliminary weak binding state and subsequent ADP release (States 3 to 4). While there may seem to be a para-
 199 dox that the transition rate between States 2 to 4 is very low, which one might interpret as the ADP released state
 200 having *low* affinity, we emphasize this quantity is a byproduct of the competing rates between physical binding
 201 and ADP capture. That is, State 2 does not have lower affinity for the microtubule, but rather, simply occurs less
 202 often than ADP rebinding. A full report of the relative proportions of each transition can be found in **Figs. S.5**
 203 **and S.6**.

204 **Binding rates can be distinctly modified by physical and chemical factors.**

205 The quantity and structure of experimental data have thus far allowed for significant progress in understanding
 206 binding from retrodictive reconciliation with a model. We conclude with predictions that emphasize the broader
 207 lessons and may serve as the basis of validation in future experiments. The exploration of typical binding events

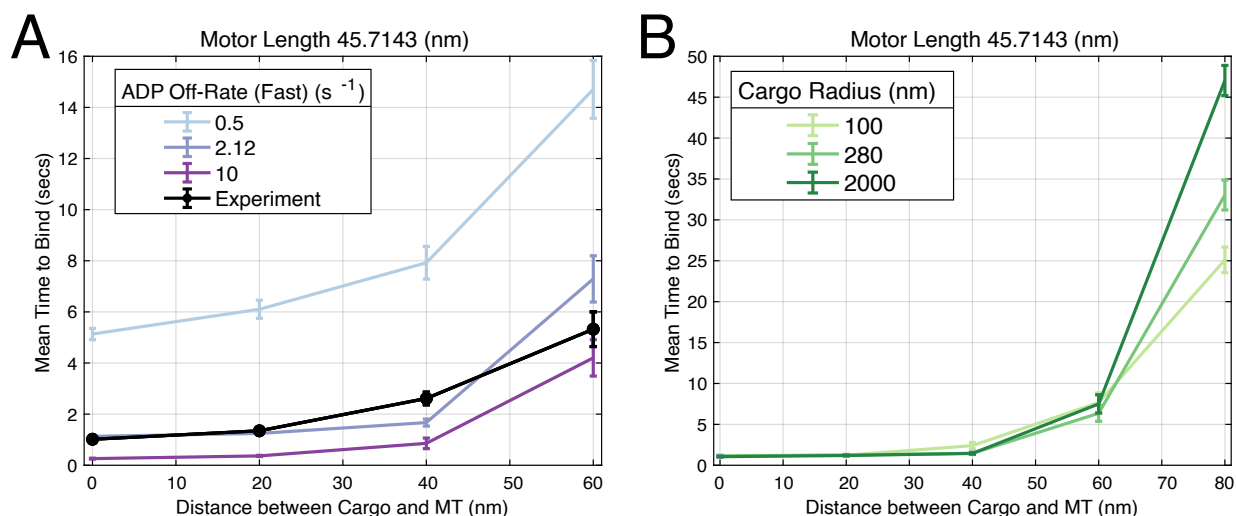


Figure 6: Predicted binding time changes from chemical and physical perturbations. **A:** An example of a chemical change, $k_{\text{off}}^{\text{ADP, Fast}}$, was varied in the simulation and resulting simulated binding times are plotted. Data are presented as mean \pm SEM. **B:** Physical changes, such as changing the cargo size, can also be made to study the resulting binding times.

208 in the previous section points toward conceptualizing this process as a distinct mechanical diffusive search and a
 209 chemical step from the nucleotide state. Regulation and perturbations of each of these components should there-
 210 fore be discernible. To explore these two scenarios, we predict how the binding times should be altered in two
 211 hypothetical experimental perturbations shown in **Fig. 6**. In the first, panel **A** shows how if one could modulate the
 212 tubulin-stimulated ADP-release rate, the effective spatially-dependent binding rate shifts up or downward for all
 213 distances. In contrast, there are numerous physical experiments that could plausibly alter the physical properties
 214 of the system. In **Fig. 6B**, we show the predicted effect of changing the cargo size, which would consequently
 215 modify the overall diffusivity of the ensemble and the random search time. For short distances that are not limited
 216 by this diffusive search, the difference is negligible, but for long distances, the effect becomes magnified. Predic-
 217 tions for other motor lengths can be found in **Fig. S.7**. While we do not currently have the technological capability
 218 to validate these experimental predictions, we hope they will be the basis of future validation or invalidation of our
 219 proposed binding model.

220 Discussion

221 Conclusion

222 Altogether, our results point toward a model of the initial binding between a cargo-bound kinesin and a microtubule
 223 track being more complex than just diffusion-limited search of the motor head presumed elsewhere [10, 31].
 224 Motivated by the known mechano-chemistry of motor stepping, where the nucleotide state of each motor head
 225 dictates microtubule affinity [36, 39, 48], we posit that the observed binding times correspond to a nucleotide-
 226 state-limited strong binding event. To validate this hypothesis, we considered a coarse-grained computational
 227 model that incorporates both diffusive search and the ADP state of motor heads, and through simulation-based
 228 inference and model selection, ultimately found compelling agreement with the experimental measurements both
 229 in the observed binding times and in agreement with estimated microscopic parameters measured elsewhere
 230 [37–41]. Even with only observed binding times, our model predicts that the "typical" binding event is modulated
 231 distinctly by both environmental and physical factors. From a design perspective, these orthogonal modulations
 232 allow for more fine-grained control and malleability than either separately.

233 Motor binding times have been estimated and measured many times prior [14–17], but these studies cannot
 234 easily disentangle the physical configuration the binding arises from, whether it be from a landing experiment,
 235 DNA origami, or motors re-attaching while another is already bound. The absence of this consideration jux-

236 tapers the increasing body of evidence that spatial organization plays a vital role in motor binding [23–26].
237 By distilling both the experimental assay and corresponding model to the minimal ingredients of a single mo-
238 tor attachment, we can clarify this process with unprecedented precision and generalizability. That is, while we
239 have shown that our model successfully recapitulates the experimental data from our optical trap assay, we have
240 moreover provided quantitative details about the underlying process that can be used to calculate binding times
241 in other configurations. That is, one could imagine taking our fitted model and adapting it to DNA-origami cargo
242 to reconcile the observed binding rates of [15, 17]. Discrepancies between the predictions and observations may
243 occur, but these provide crucial details about the underlying chemistry and physics that we advocate warrant
244 further investigation.

245 **Limitations and Assumptions**

246 We have not, and likely cannot ever fully rule out other conceptual models and confounding factors of binding
247 time. The key qualitative feature we sought to replicate was the binding delay on the order of 1 second in close-
248 proximity cargoes. Our ADP release model successfully recapitulates this, and we provide testable hypotheses
249 that can be used to invalidate the model in **Fig. 6**. We considered several other possible factors that may explain
250 or contribute to this delay. The most pressing possibility is whether this delay arises as an artifact of failure to
251 detect optical trap displacements faster than this. Assuming an unloaded kinesin velocity of around 500 nm/s, a
252 15 nm bead displacement for detection corresponds to fractions of a second, and does not explain the observed
253 delay on the order of a second. In our model, we assumed the motor was configured downward initially, but this is
254 likely not the case. However, based on the estimates of a cargo taking 0.2 seconds to complete a full rotation at
255 this viscosity [26], we do not believe this can explain the delay. Furthermore, we are unsure what a realistic initial
256 configuration of the motor may be, as a more detailed model of the cargo resetting in the optical trap likely requires
257 consideration of hydrodynamic effects that couple rotation and motion and distant-dependent diffusivity [49]. One
258 last possibility we note is the conceptual model where a motor begins in a "crumpled" state, and then unfurls with
259 some delay to bind. Our model of the kinesin stalk is crude, and one could imagine other possibilities such as
260 a worm-like chain model considered for the neck linker [50]. However, these models primarily differ when under
261 load, rather than undergoing a diffusive search. Therefore, we leave the investigation of other polymer models
262 for the stalk to future work. We note the coarse-grained approximation of the whole motor head as a single
263 spatial point with a single nucleotide state. We also leave to future work more detailed models with two distinct
264 motor heads, as we do not believe this would greatly change the qualitative lessons emerging from our work.
265 Lastly, we identify that this binding model may be limited to kinesin, and perhaps even only some kinesins. Future
266 investigation warrants investigating other motors binding details, e.g., dynein, through the procedure outlined in
267 this work.

268 **Context in Cytoskeletal-Motor Systems**

269 The focus of this work is understanding the binding between a single cargo-bound kinesin and a microtubule track.
270 This setup follows the spirit of a now long-established and successful line of investigation of cytoskeletal-motor
271 assemblies by isolating fundamental building blocks. We attempt to situate our advances in the broader context
272 of the wildly complex array of cytoskeletal-motor interactions and the feedback between them. We emphasize
273 the chemo-mechanical nature of our binding model in the context of the enormous literature on how physical
274 and chemical changes to microtubules affect motor behavior. For instance, geometry of the microtubule network
275 dictates cargo-microtubule distances [51, 52], and motors themselves reorganize microtubules through forces
276 [31]. A zoo of microtubule-associating-proteins (MAPs) and the tubulin code are known to interfere with motor
277 function [53, 54], including in the recruitment of motors [55–57]. Our model may shed light on explaining the
278 mechanisms by which these microtubule decorations modify motor binding, and serve as the basis for future
279 investigation. Through the decomposition of how chemical and physical factors modulate binding, our study may
280 be the basis for discerning the mechanism of MAPs regulation of motors. For instance, one could imagine C-
281 terminal tails may serve as physical tethers or may alter nucleotide states, and such an investigation remains for
282 the future. More broadly, this understanding serves as a key step toward understanding how cells regulate binding
283 to direct cargo and perform even more cytoskeletal-motor functions such as coordinate mitosis [58]. Moreover,
284 this understanding may help aid in the design of increasingly sophisticated synthetic systems [59], where spatial
285 distances can be prescribed.

286 **Broader Lessons for Probing Protein-Protein Interactions**

287 The difficulty in directly observing protein-protein interactions makes their study challenging. Two main avenues
288 of approaches have been historically successful, each at extremes of chosen level of detail. Molecular dynamics
289 simulations are a gold standard for predicting interactions. We build on the immense insight they have illuminated
290 on the interactions between microtubules and kinesin [60, 61] and otherwise would not have considered the ADP
291 release in our model. However, these approaches built from microscopic components have immense difficulty
292 in scaling up to more complex systems with multiple interacting components, such as between motor, cargo,
293 and cytoskeletal filaments. At the other extreme, "spherical cow" models of diffusion-limited reactions [62, 63]
294 have revealed many qualitative lessons of protein-protein interactions, but remain challenging to quantitatively link
295 with data because even the inclusion of modest complexities like orientation constraints [64] make the analyses
296 prohibitively complex.

297 Our work adds a timely vignette to other studies [65, 66] that illustrates the value of striking an intermediate
298 level of complexity in understanding protein-protein interactions. This balance allows for the incorporation of
299 microscopic details from more fine-grained studies, but remains vigilantly coarse-grained to directly connect with
300 data. We highlight major components of the work that we believe will be of broader use in other probing of protein-
301 protein interactions. For one, we leveraged measuring interactions in a variety of conditions. Equipped with only a
302 single motor length or trapped distance, the diffusion model would have fit to a seemingly satisfactory degree. By
303 probing a model's ability to explain data across conditions, we were able to identify the ADP model. Furthermore,
304 our work was made possible by recent advances in simulation-based inference [67]. While model fitting has
305 historically been bogged down in the complications of the procedure, we now live in an age where it is plausible
306 to perform inference on any model that can be thought of (and simulated), with rapidly improving techniques
307 beyond those we utilized in this work [68]. Neither of these lessons is specific to the context of cytoskeletal-
308 motor interactions, and therefore we hope serves as an outline for other pursuits in data-driven discovery of
309 protein-protein interactions.

310 **Material and Methods**

311 **Optical Trap Experiments**

312 The optical trapping setup was assembled on an inverted Nikon TE200 microscope using a 980 nm, single mode,
313 fiber-coupled diode laser (EM4 Inc). The laser power was set to achieve a trap stiffness, κ_t , of ~ 0.045 pN nm⁻¹
314 while using the polystyrene bead of 0.56 μ m (streptavidin conjugated, Spherotech).

315 Single motor experiments were carried out in the motility buffer (80 mM Pipes pH 6.9, 50 mM CH3COOK,
316 4 mM MgSO4, 1 mM DTT, 1 mM EGTA, 10 μ M taxol, 1 mg mL⁻¹ casein). In all the rebinding rate assays,
317 single-motor kinesin-coated polystyrene beads were prepared just before the measurements. The motors DK-
318 406-His/K-560-His/DK-746-His (Kinesin-1, aa 1-560/Drosophila Kinesin aa 1-406/ Drosophila Kinesin aa 1-746;
319 His tag at c-term) were diluted to ~ 20 nM before mixing with ~ 1 pM of biotinylated penta-His- antibody conjugated
320 streptavidin beads stored at 4°C. This ratio produced the bead binding fraction of 10-15% and was maintained
321 to maximize the probability of finding single motor beads in the solution. The bead-motor incubation (~ 50 μ L
322 volume) was carried out at room temperature for 10 minutes. At the end of incubation, the sample chamber with
323 preassembled microtubules was washed with ~ 50 μ L of warm filtered buffer just before injecting the incubated
324 mixture. Experiments were carried out at room temperature in a motility buffer supplemented with 2 mM ATP and
325 oxygen-scavenging system (0.25 mg mL⁻¹ glucose oxidase, 30 μ g mL⁻¹ catalase, 4.5 mg mL⁻¹ glucose).

326 In general, small dust or debris in the solution gets pulled into the trap along with the bead. Trapped dust
327 interferes with motor rebinding to microtubules. To prevent this interference, the large dust particles and aggre-
328 gates of casein in the buffer were removed using a 100 nm centrifugal filter (Millipore). Another potential issue is
329 the stage drift during measurement, and it was minimized with an automated drift correction system using an xyz
330 piezo stage (PI) and custom software.

331 All kinesin proteins were purified using HIS-tag and MT affinity purification after expressing them in Rosetta
332 bacterial cells as described earlier [69]. DK406 plasmid was procured from Addgene (plasmid ID #129764,
333 generously supplied by William Hancock lab). DK746 was designed in the lab after modifying the full-length
334 DK980, also procured from Addgene (plasmid ID: #129762, William Hancock lab), using restriction enzyme
335 digestion.

336 Binding Detection

337 Bead displacements in the trap registered by a position-sensitive diode (PSD; First Sensor AG) were acquired at
 338 3kHz using an analog-to-digital converter (ADC) card. The digitized PSD data was smoothed with a 40 point fast
 339 Fourier transform (FFT) filter and analyzed by custom Matlab code to score all the peaks greater than 15 nm and
 340 lasting more than 0.01 seconds (30 data points). The experimental method is fully described in [70].

341 Brownian Dynamics Simulation

342 The simulation consists of a motor that is bound to a cargo and a microtubule. The cargo is a three-dimensional
 343 sphere and is subject to translational and rotational diffusion. The motor's condition is dependent on whether an
 344 ADP molecule is bound to it and whether it is bound to the microtubule. Whether the motor is weakly or strongly
 345 bound to the microtubule is dependent on whether it is bound to an ADP molecule. The transitions through
 346 these states (**Fig. 2**) are simulated using a Gillespie-style algorithm [71]. The motor is defined by its location
 347 of attachment to the cargo and its head location. Locations of the motor head and cargo center are calculated
 348 using the Euler-Maruyama method [72]. When the motor heads comes within binding reach of the microtubule, it
 349 has a constant rate of binding to it; otherwise, this rate is 0. The motor behaves as a spring, and when they are
 350 bound, they experience and exert force. When the motor is weakly bound to the microtubule, its off-rate depends
 351 on force. ADP molecules can also bind and unbind to the motor head at constant rates, but the ADP off-rate
 352 is dependent on whether the motor is weakly bound to the microtubule. The equations of motion for the cargo
 353 and motor are constructed by discretizing a set of stochastic ordinary differential equations derived from force
 354 balance.

355 ADP Release Model Description

356 This model is three-dimensional and mesoscale. A set of stochastic ordinary differential equations is used to
 357 describe the location of the cargo sphere and the motor that is attached to it. The motor transitions stochastically
 358 between discrete states (**Fig. 2**), and these transitions occur as Poisson processes. The force that the motor
 359 exerts on the cargo is modeled as a one-way spring:

$$\vec{F}^m(\vec{a}, \vec{h}) = \begin{cases} -\kappa^m (|\vec{h} - \vec{a}| - L_m) \left(\frac{\vec{h} - \vec{a}}{|\vec{h} - \vec{a}|} \right) + \vec{F}^w & |\vec{h} - \vec{a}| > L_m \\ 0 & |\vec{h} - \vec{a}| \leq L_m \end{cases}, \quad (1)$$

360 where \vec{a} and \vec{h} are the motor anchor and head locations, respectively, κ^m is the motor stiffness constant, L_m is
 361 the motor rest length,

$$\vec{F}^w = \begin{cases} \kappa^w (\vec{a}_{MT} - \vec{h}) & \text{motor is weakly bound to the microtubule} \\ 0 & \text{motor is unbound from the microtubule} \end{cases}, \quad (2)$$

362 κ^w is the weak spring between the motor head and the microtubule, and \vec{a}_{MT} is where the motor head is weakly
 363 bound on the microtubule. There is a torque that is exerted on the cargo:

$$\vec{\tau}^m(\vec{a}, \vec{h}, \vec{c}) = \begin{cases} (\vec{a} - \vec{c}) \times \vec{F}^m(\vec{a}, \vec{h}) & \text{motor is weakly bound to the microtubule} \\ 0 & \text{otherwise} \end{cases}, \quad (3)$$

364 where \vec{c} is the cargo center location. Thus, we have ordinary differential equations (modeled after the Langevin
 365 equation):

$$\frac{d\vec{c}(t)}{dt} = \frac{1}{6\pi\eta R} \vec{F}^m(\vec{a}(t), \vec{h}(t)) + \frac{1}{6\pi\eta R} \vec{F}^b(t), \quad (4)$$

366 and

$$\frac{d\vec{\theta}(t)}{dt} = \frac{1}{8\pi\eta R^3} \vec{\tau}^m(\vec{a}(t), \vec{h}(t), \vec{c}(t)) + \frac{1}{8\pi\eta R^3} \vec{\tau}^b(t), \quad (5)$$

367 where η is the water viscosity, R is the cargo sphere radius, θ is the cargo orientation, and \vec{F}^b and $\vec{\tau}^b$ are the
 368 Brownian force and torque, respectively, which are random variables with mean 0 and variance $2k_B T \xi_c$, and ξ_c
 369 is the drag coefficient of the cargo. According to the Euler-Maruyama method, a discrete formulation of **Eqs. (4)**
 370 **and (5)** will be:

$$\vec{c}(t_{n+1}) = \vec{c}(t_n) + \frac{1}{6\pi\eta R} \vec{F}^m(\vec{a}(t_n), \vec{h}(t_n)) \Delta t + \sqrt{2 \frac{k_B T}{6\pi\eta R} \Delta t} \vec{G}_c(t_n) \quad (6)$$

371 and

$$\vec{\theta}(t_{n+1}) = \vec{\theta}(t_n) + \frac{1}{8\pi\eta R^3} \vec{\tau}^m(\vec{a}(t_n), \vec{h}(t_n), \vec{c}(t_n)) \Delta t + \sqrt{2 \frac{k_B T}{8\pi\eta R^3} \Delta t} \vec{G}_\theta(t_n), \quad (7)$$

372 where n is the current time step, and \vec{G}_c and \vec{G}_θ are mutually uncorrelated vectors of independent and identically
 373 distributed (i.i.d.) Gaussian random variables with mean 0 and variance 1. The cargo cannot phase through the
 374 microtubule. Since we are simulating optical trap experiments, we add a force from the trap on the cargo:

$$\vec{c}(t_{n+1}) = \vec{c}(t_n) + \kappa_t (\vec{c}(1) - \vec{c}(t_n)) + \frac{1}{6\pi\eta R} \vec{F}^m(\vec{a}(t_n), \vec{h}(t_n)) \Delta t + \sqrt{2 \frac{k_B T}{6\pi\eta R} \Delta t} \vec{G}_c(t_n), \quad (8)$$

375 where κ_t is the trap stiffness. We can now determine the motor anchor location by inputting the cargo axis of
 376 rotation $\vec{\theta}(t_{n+1}) - \vec{\theta}(t_n)$ and this axis' length as the magnitude of rotation (in radians) into a rotation matrix
 377 $\mathbf{M}(t_n)$:

$$\vec{a}(t_{n+1}) = \mathbf{M}(t_n) (\vec{a}(t_n) - \vec{c}(t_n)) + \vec{c}(t_n) + (\vec{c}(t_{n+1}) - \vec{c}(t_n)). \quad (9)$$

378 Similarly to **Eqs. (4) and (5)**, we discretize ordinary differential equations for the motor head position:

$$\vec{h}(t_{n+1}) = \vec{h}(t_n) + \frac{1}{\xi_m} \vec{F}^m \Delta t + \sqrt{2D_m} \vec{G}_m, \quad (10)$$

379 where $\xi_m = k_B T / D_m$ is the motor drag coefficient, D_m is the motor head diffusion constant, and \vec{G}_m is the
 380 uncorrelated i.i.d. Gaussian random variable of mean 0 and variance 1. The motor head cannot phase through
 381 the microtubule and the cargo. Since in experiments, the microtubule lies on the coverslip surface, the motor
 382 head cannot diffuse under the microtubule.

383 Transitions between each motor state (**Fig. 2**) are modeled as Poisson processes, with rates as follows:

$$\lambda_{\text{off}}^{\text{ADP}} = \begin{cases} k_{\text{off}}^{\text{ADP}} & \text{motor is ADP-bound and unbound from the microtubule} \\ k_{\text{off}}^{\text{ADP, Fast}} & \text{motor is ADP-bound and weakly bound to the microtubule} \\ 0 & \text{motor is ADP-unbound} \end{cases} \quad (11)$$

$$\lambda_{\text{on}}^{\text{ADP}} = \begin{cases} k_{\text{on}}^{\text{ADP}} & \text{motor is ADP-unbound} \\ 0 & \text{motor is ADP-bound} \end{cases} \quad (12)$$

$$\lambda_{\text{on}}^{\text{MT}} = \begin{cases} k_{\text{on}}^{\text{MT}} & \text{motor is unbound from microtubule and within } d_{\text{MT}} \\ k_{\text{off}}^{\text{ADP, Fast}} & \text{motor is weakly bound to microtubule} \\ 0 & \text{motor is not within } d_{\text{MT}} \end{cases}, \quad (13)$$

384 where d_{MT} is the binding distance between the motor head and the microtubule, and

$$\lambda_{\text{off}}^{\text{MT}} = \begin{cases} k_{\text{off}}^{\text{MT}} \cdot \exp F^w / F^d & \text{motor is weakly bound to the microtubule} \\ 0 & \text{motor is MT-unbound} \end{cases}, \quad (14)$$

385 where F^d is the motor's critical detachment force. Parameter values are listed in **Tables 1 and 2**.

386

Parameter	Description	Value
κ^m	Motor stiffness constant (pN/nm) [12]	0.3200
κ_t	Trap Stiffness (pN/nm) [†]	[0.045 0.045 0.03]
L_m	Motor length (nm) [†]	Varies
η	Viscosity of experimental fluid (pN · s/nm ²)	1e-05
R	Radius of experimental cargo bead (nm)	280
$k_b T$	Boltmann constant (pN · nm)	4.114
d_{MT}	Binding range between MT and motor head (nm)*	5
F^d	Motor critical detachment force (pN) [19]	4

Table 2: Measured parameters. *Unmeasured estimate. [†]Measured estimate. The motor length includes the antibody that binds the motor to the cargo (about 10 nm).

Initial Conditions

The simulation begins with the cargo d nm away from the microtubule, the latter of which does not move during the entire simulation (**Fig. S.1a**). The motor is anchored at the bottom of the cargo and is vertically straight, based on the fast reset back to the trap center. If there is not enough space ($d < L_m$), then the motor head and cargo are initialized to the top of the microtubule.

Numerical Simulation

The model is simulated forward in time. Time steps are either equal to dt_{\max} , the maximum time step the system can undergo, or they are determined through the Gillespie-style algorithm if the next motor state-change event (i.e., bound or unbound to microtubule, ADP released or unreleased), also determined by the Gillespie-style algorithm, occurs before $t_n + dt_{\max}$. An appropriate dt_{\max} (0.004) was chosen with a convergence test (**Fig. S.8**). To implement the Gillespie-style algorithm, exponential random variables from distributions with means set by each Poisson (**Eqs. (11) to (14)**) were generated at each time step. After the Gillespie-style algorithm determines the next event and when it occurs, the time step is used to determine the locations of the cargo center and the motor's head and anchor (**Eqs. (8) to (10)**).

To mimic experimental practices, simulations are allowed to simulate 100 seconds. If the motor does not strongly bind to the microtubule during this time, the simulation starts over. This method is similar to the experiment, where the assay is run for 100 seconds screening for a binding event to occur before trapping a different cargo. The simulation is written in MATLAB, and takes approximately 0.1 seconds to simulate 1 second of the system. Example snapshots of the simulation are shown in **Fig. S.1**.

Model Fitting, Cross-Validation

The model is fit through two distinct approximate inference procedures, the reconciliation of which serves as a validation for the approximations. The first procedure is a Bayesian optimization procedure [27] to obtain a single point estimate for the parameter values. The loss function is the squared distance over the mean binding times (and therefore neglects the full distributional information) and the estimated mean binding time over $S = 1000$ simulations, and these estimates are used in **Fig. 3** and **Table 1**.

To obtain uncertainty quantification seen in **Fig. 4**, we also employ a sequential Monte Carlo approximate Bayesian computation approach [28]. These techniques are far slower than the optimization procedure and require the specification of a prior distribution for each parameter, but provide some notion of uncertainty quantification, and were used to generate **Fig. 4** with some data withheld. That is, because of the heavy computation expense, only the shortest motor at 0 nm average distance between the cargo and microtubule, the mid-length motor at 40 nm average distance, and the longest motor at 80 nm average distance were used in the fitting. The maximum a posteriori (MAP) estimates from this latter procedure closely agree those of the first procedure, supporting the validity of both. Furthermore, in **Table S.1**, we show the inference procedures successfully infer rates from synthetic data. Lognormal priors are chosen for all parameters, and hyperparameters are shown in **Table 3**. Initially, 100 simulations estimate the binding times in the model, and weights in the sequential Monte

422 Carlo algorithm are defined as $w_i = \frac{\pi}{\sum w_{i-1} K_i}$, where K_i is the perturbation kernel for the i th sequence, $i > 1$.
423 We use a Gaussian distribution for K . These new samples are then used to simulate more mean binding times,
424 until 100 samples are generated that resulted in a relative error lower than 1.8. Eight more sequences follow in
425 this same manner, each time the relative error threshold decreases by 0.2. A kernel density estimator was then
426 applied to the resulting samples shown in **Fig. 4**.

Parameter	Mean	Standard Deviation
$k_{\text{off}}^{\text{ADP}}$	10^{-2}	0.001
$k_{\text{on}}^{\text{ADP}}$	10^3	100
$k_{\text{off}}^{\text{ADP, Fast}}$	$10^{0.3}$	1
$k_{\text{on}}^{\text{MT}}$	$10^{1.7}$	100
$k_{\text{off}}^{\text{MT}}$	10^{-1}	0.01
D_m	$10^{3.3}$	100
κ_w	$10^{-2.7}$	0.001

Table 3: Hyperparameters for priors used in estimated posterior densities, all taken to be lognormal distributions.

427 The cross-validation procedure in **Fig. 3** was implemented by fitting the models using the aforementioned
428 point estimate optimization scheme with data withheld, and then test error defined to be $N^{-1} \sum_{i=1}^N (t_i - \hat{t}_i)/t_i$,
429 a percentage error over the test scenarios. This procedure is validated in **Fig. S.9** that shows cross-validation
430 successfully identifying the correct model when tested against synthetic data.

431 Software Availability

432 MATLAB code to reproduce our results (compatible with version R2020a) is available at [https://github.com/
433 trininguyen/MotorBinding/tree/master](https://github.com/trininguyen/MotorBinding/tree/master).

434 Acknowledgements

435 This work was supported by the National Science Foundation Graduate Research Fellowship under Grant No.
436 DGE-1839285 and the National Institutes of Health under Grant R01 GM123068. **Figure 2** includes an icon
437 (lipid-hdl-1 icon) by Servier <https://smart.servier.com/>, which is licensed under CC-BY 3.0 Unported. This
438 work utilized the infrastructure for high-performance and high-throughput computing, research data storage and
439 analysis, and scientific software tool integration built, operated, and updated by the Research Cyberinfrastructure
440 Center (RCIC) at the University of California, Irvine (UCI). The RCIC provides cluster-based systems, application
441 software, and scalable storage to directly support the UCI research community. <https://rcic.uci.edu>.

442 References

- 443 [1] G. Schreiber, G. Haran, and H.-X. Zhou. "Fundamental aspects of protein- protein association kinetics". *Chemical reviews* 109.3
444 (2009), pp. 839–860.
- 445 [2] L. Mabonga and A. Kappo. "Protein-protein interaction modulators: advances, successes and remaining challenges". *Biophysical Re-*
446 *views* (2019).
- 447 [3] G. Schreiber and A. E. Keating. "Protein binding specificity versus promiscuity". *Current opinion in structural biology* 21.1 (2011),
448 pp. 50–61.
- 449 [4] K. Titeca, I. Lemmens, J. Tavernier, and S. Eyckerman. "Discovering cellular protein-protein interactions: technological strategies and
450 opportunities". *Mass Spectrometry Reviews* (2018).
- 451 [5] C. Rakers, M. Bermudez, B. G. Keller, J. Mortier, and G. Wolber. "Computational close up on protein–protein interactions: how to
452 unravel the invisible using molecular dynamics simulations?" *Wiley Interdisciplinary Reviews: Computational Molecular Science* 5.5
453 (2015), pp. 345–359.
- 454 [6] B. Grafstein and D. Forman. "Intracellular Transport in Neurons". *Physiological Reviews* (1980).

- 455 [7] L. Wordeman. "How kinesin motor proteins drive mitotic spindle function: Lessons from molecular assays". *Seminars in Cell & Developmental Biology*. Vol. 21. 3. Elsevier. 2010, pp. 260–268.
- 456
- 457 [8] I. Tikhonenko, V. Magidson, R. Gräf, A. Khodjakov, and M. P. Koonce. "A kinesin-mediated mechanism that couples centrosomes to
458 nuclei". *Cellular and Molecular Life Sciences* 70 (2013), pp. 1285–1296.
- 459 [9] V. C. Nadar, A. Ketschek, K. A. Myers, G. Gallo, and P. W. Baas. "Kinesin-5 is essential for growth-cone turning". *Current Biology* 18.24
460 (2008), pp. 1972–1977.
- 461 [10] Z. Zhang, N. Danne, B. Meddens, and J. Erwin. "Direct imaging of intraflagellar-transport turnarounds reveals that motors detach,
462 diffuse, and reattach to opposite-direction trains". *PNAS* (2021).
- 463 [11] T. Nishizaka, H. Miyata, H. Yoshikawa, S. Ishiwata, and K. Kinoshita Jr. "Unbinding force of a single motor molecule of muscle measured
464 using optical tweezers". *Nature* (1995).
- 465 [12] H. Kojima, E. Muto, H. Higuchi, and T. Yanagida. "Mechanics of single kinesin molecules measured by optical trapping nanometry".
466 *Biophysical Journal* (1997).
- 467 [13] A. Seitz, H. Kojima, K. Oiwa, E.-M. Mandelkow, Y.-H. Song, and E. Mandelkow. "Single-molecule investigation of the interference
468 between kinesin, tau and MAP2c". *The EMBO journal* 21.18 (2002), pp. 4896–4905.
- 469 [14] H. Palacci, O. Idan, M. J. Armstrong, A. Agarwal, T. Nitta, and H. Hess. "Velocity fluctuations in kinesin-1 gliding motility assays originate
470 in motor attachment geometry variations". *Langmuir* 32.31 (2016), pp. 7943–7950.
- 471 [15] Q. Feng, K. J. Mickolajczyk, G.-Y. Chen, and W. O. Hancock. "Motor reattachment kinetics play a dominant role in multimotor-driven
472 cargo transport". *Biophysical journal* 114.2 (2018), pp. 400–409.
- 473 [16] J. Xu, Z. Shu, S. J. King, and S. P. Gross. "Tuning multiple motor travel via single motor velocity". *Traffic* 13.9 (2012), pp. 1198–1205.
- 474 [17] K. Furuta, A. Furuta, Y. Y. Toyoshima, M. Amino, K. Oiwa, and H. Kojima. "Measuring collective transport by defined numbers of
475 processive and nonprocessive kinesin motors". *Biophysical Journal* 104.2 (2013), 383a.
- 476 [18] C. Leduc, O. Campàs, K. B. Zeldovich, A. Roux, P. Jolimaitre, L. Bourel-Bonnet, B. Goud, J.-F. Joanny, P. Bassereau, and J. Prost.
477 "Cooperative extraction of membrane nanotubes by molecular motors". *Proceedings of the National Academy of Sciences* 101.49
478 (2004), pp. 17096–17101.
- 479 [19] A. Kunwar, S. Tripathy, J. Xu, M. Mattson, P. Anand, R. Sigua, M. Vershinin, R. McKenney, C. Yu, A. Mogilner, and S. Gross. "Mechanical
480 stochastic tug-of-war models cannot explain bidirectional lipid-droplet transport". *PNAS* (2011).
- 481 [20] S. Klumpp and R. Lipowsky. "Cooperative cargo transport by several molecular motors". *The Proceedings of the National Academy of
482 Sciences* (2005).
- 483 [21] C. Miles, S. Lawley, and J. Keener. "Analysis of Nonprocessive molecular motor transport using renewal reward theory". *SIAM Journal
484 on Applied Mathematics* (2018).
- 485 [22] C. Miles and J. Keener. "Bidirectionality from cargo thermal fluctuations in motor-mediated transport". *Journal of Theoretical Biology*
486 (2017).
- 487 [23] Q. Li, K.-F. Tseng, S. J. King, W. Qiu, and J. Xu. "A fluid membrane enhances the velocity of cargo transport by small teams of
488 kinesin-1". *Biophysical Journal* 114.3 (2018), 509a.
- 489 [24] N. Sarpangala and A. Gopinathan. "Cargo surface fluidity can reduce inter-motor mechanical interference, promote load-sharing and
490 enhance processivity in teams of molecular motors". *PLOS Computational Biology* 18.6 (2022), e1010217.
- 491 [25] S. Yadav and A. Kunwar. "Sliding of motor tails on cargo surface due to drift and diffusion affects their team arrangement and collective
492 transport". *Physical Biology* 20.1 (2022), p. 016002.
- 493 [26] M. Bovyn, B. Narayanareddy, S. Gross, and J. Allard. "Diffusion of kinesin motors on cargo can enhance binding and run lengths
494 during intracellular transport". *Molecular Biology of the Cell* (2021).
- 495 [27] L. Acerbi and W. Ma. "Practical Bayesian optimization for model fitting with Bayesian Adaptive Direct Search". *Advances in Neural
496 Information Processing Systems* (2017).
- 497 [28] S. Sisson, Y. Fan, and M. Tanaka. "Sequential Monte Carlo without likelihoods". *PNAS* (2007).
- 498 [29] D. J. Warne, R. E. Baker, and M. J. Simpson. "Rapid Bayesian inference for expensive stochastic models". *Journal of Computational
499 and Graphical Statistics* 31.2 (2022), pp. 512–528.
- 500 [30] Z. Zhang, Y. Goldtzvik, and D. Thirumalai. "Parsing the roles of neck-linker docking and tethered head diffusion in the stepping dynamics
501 of kinesin". *Proceedings of the National Academy of Sciences* 114.46 (2017), E9838–E9845.
- 502 [31] W. Yan, S. Ansari, A. Lamson, M. A. Glaser, R. Blackwell, M. D. Betterton, and M. Shelley. "Toward the cellular-scale simulation of
503 motor-driven cytoskeletal assemblies". *Elife* 11 (2022), e74160.
- 504 [32] S. Uemura, K. Kawaguchi, J. Yajima, M. Edamatsu, Y. Y. Toyoshima, and S. Ishiwata. "Kinesin–microtubule binding depends on both
505 nucleotide state and loading direction". *Proceedings of the National Academy of Sciences* 99.9 (2002), pp. 5977–5981.
- 506 [33] R. A. Cross. "The kinetic mechanism of kinesin". *Trends in biochemical sciences* 29.6 (2004), pp. 301–309.
- 507 [34] A. B. Asenjo, Y. Weinberg, and H. Sosa. "Nucleotide binding and hydrolysis induces a disorder-order transition in the kinesin neck-linker
508 region". *Nature structural & molecular biology* 13.7 (2006), pp. 648–654.
- 509 [35] B. Milić, J. Andreasson, W. Hancock, and S. Block. "Kinesin processivity is gated by phosphate release". *The Proceedings of the
510 National Academy of Science* (2014).

- 511 [36] D. Hackney. "Kinesin ATPase: rate-limiting ADP release". *PNAS* (1988).
- 512 [37] T. Shimizu, E. Sablin, R. Vale, R. Fletterick, E. Pechatnikova, and E. Taylor. "Expression, purification, ATPase properties, and microtubule-
513 binding properties of the ncd motor domain". *American Chemical Society* (1995).
- 514 [38] W. Hancock and J. Howard. "Kinesin's processivity results from mechanical and chemical coordination between the ATP hydrolysis
515 cycles of the two motor domains". *PNAS* (1999).
- 516 [39] D. Hackney and M. Stock. "Kinesin's IAK tail domain inhibits initial microtubule-stimulated ADP release". *Nature Cell Biology* (2000).
- 517 [40] T. Shimizu, K. Thorn, A. Ruby, and R. Vale. "ATPase kinetic characterization and single molecule behavior of mutant human kinesin
518 motors defective in microtubule-based motility". *American Chemical Society* (2000).
- 519 [41] C. Friel and J. Howard. "The kinesin-13 MCAK has an unconventional ATPase cycle adapted for microtubule depolymerization". *The
520 EMBO Journal* (2011).
- 521 [42] Z. Zhang, Y. Goldtzvik, and D. Thirumalai. "Parsing the roles of neck-linker docking and tethered head diffusion in the stepping dynamics
522 of kinesin". *PNAS* (2017).
- 523 [43] K. P. Burnham and D. R. Anderson. "Multimodel inference: understanding AIC and BIC in model selection". *Sociological methods &
524 research* 33.2 (2004), pp. 261–304.
- 525 [44] J. Liepe, P. Kirk, S. Filippi, T. Toni, C. P. Barnes, and M. P. Stumpf. "A framework for parameter estimation and model selection from
526 experimental data in systems biology using approximate Bayesian computation". *Nature protocols* 9.2 (2014), pp. 439–456.
- 527 [45] P. Zhang. "Model selection via multifold cross validation". *The annals of statistics* (1993), pp. 299–313.
- 528 [46] W. Hancock and J. Howard. "Processivity of the motor protein kinesin requires two heads". *Journal of Cell Biology* (1998).
- 529 [47] P. Hill. "Kernel estimation of a distribution function". *Communication in Statistics - Theory and Methods* (1985).
- 530 [48] S. Block. "Kinesin Motor Mechanics: Binding, Stepping, Tracking, Gating, and Limping". *Biophysical Journal* (2007).
- 531 [49] B. Sprinkle, E. B. Van Der Wee, Y. Luo, M. M. Driscoll, and A. Donev. "Driven dynamics in dense suspensions of microrollers". *Soft
532 Matter* 16.34 (2020), pp. 7982–8001.
- 533 [50] M. L. Kutys, J. Fricks, and W. O. Hancock. "Monte Carlo analysis of neck linker extension in kinesin molecular motors". *PLoS compu-
534 tational biology* 6.11 (2010), e1000980.
- 535 [51] M.-V. Ciocanel, B. Sandstede, S. P. Jeschonek, and K. L. Mowry. "Modeling microtubule-based transport and anchoring of mRNA".
536 *SIAM journal on applied dynamical systems* 17.4 (2018), pp. 2855–2881.
- 537 [52] S. Mogre, J. Christensen, S. Reck-Peterson, and E. Koslover. "Optimizing microtubule arrangements for rapid cargo capture". *Biophys-
538 ical Journal* (2021).
- 539 [53] C. Janke and M. Magiera. "The tubulin code and its role in controlling microtubule properties and functions". *Nature Reviews: Molecular
540 Cell Biology* (2020).
- 541 [54] M. Sirajuddin, L. Rice, and R. Vale. "Regulation of microtubule motors by tubulin isoforms and post-translational modifications". *Nature
542 Cell Biology* (2014).
- 543 [55] P. J. Hooikaas, M. Martin, T. Mühlethaler, G.-J. Kuijntjes, C. A. Peeters, E. A. Katrukha, L. Ferrari, R. Stucchi, D. G. Verhagen, W. E.
544 Van Riel, et al. "MAP7 family proteins regulate kinesin-1 recruitment and activation". *Journal of Cell Biology* 218.4 (2019), pp. 1298–
545 1318.
- 546 [56] D. Lessard, O. Zinder, T. Hotta, and K. Verhey. "Polyglutamylation of tubulin's C-terminal tail controls pausing and motility of kinesin-3
547 family member KIF1A". *Journal of Biological Chemistry* (2019).
- 548 [57] X. Fan and R. J. McKenney. "Control of motor landing and processivity by the CAP-Gly domain in the KIF13B tail". *Nature Communi-
549 cations* 14.1 (2023), p. 4715.
- 550 [58] K. M. Ori-McKenney and R. J. McKenney. "Tau oligomerization on microtubules in health and disease". *Cytoskeleton* (2023).
- 551 [59] G. Saper and H. Hess. "Synthetic systems powered by biological molecular motors". *Chemical reviews* 120.1 (2019), pp. 288–309.
- 552 [60] A. Pan, A. Pan, B. Brooks, and X. Wu. "Molecular Simulation Study on the Walking Mechanism of Kinesin Dimers on Microtubules".
553 *Current Advances in Chemistry and Biochemistry* (2021).
- 554 [61] X.-X. Shi, Y.-B. Fu, S.-K. Guo, P.-Y. Wang, H. Chen, and P. Xie. "Investigating role of conformational changes of microtubule in regulating
555 its binding affinity to kinesin by all-atom molecular dynamics simulation". *Proteins: Structure, Function, and Bioinformatics* 86.11 (2018),
556 pp. 1127–1139.
- 557 [62] A. Szabo, K. Schulten, and Z. Schulten. "First passage time approach to diffusion controlled reactions". *The Journal of chemical
558 physics* 72.8 (1980), pp. 4350–4357.
- 559 [63] P. Hänggi, P. Talkner, and M. Borkovec. "Reaction-rate theory: fifty years after Kramers". *Reviews of modern physics* 62.2 (1990),
560 p. 251.
- 561 [64] O. Berg. "Orientation constraints in diffusion-limited macromolecular association. The role of surface diffusion as a rate-enhancing
562 mechanism". *Biophysical journal* 47.1 (1985), pp. 1–14.
- 563 [65] N. N. Batada, L. A. Shepp, and D. O. Siegmund. "Stochastic model of protein–protein interaction: Why signaling proteins need to be
564 colocalized". *Proceedings of the National Academy of Sciences* 101.17 (2004), pp. 6445–6449.
- 565 [66] J. Goyette, C. S. Salas, N. Coker-Gordon, M. Bridge, S. A. Isaacson, J. Allard, and O. Dushek. "Biophysical assay for tethered signaling
566 reactions reveals tether-controlled activity for the phosphatase SHP-1". *Science advances* 3.3 (2017), e1601692.

- 567 [67] K. Cranmer, J. Brehmer, and G. Louppe. "The frontier of simulation-based inference". *Proceedings of the National Academy of Sci-*
568 *ences* 117.48 (2020), pp. 30055–30062.
- 569 [68] J.-M. Lueckmann, J. Boelts, D. Greenberg, P. Goncalves, and J. Macke. "Benchmarking simulation-based inference". *International*
570 *conference on artificial intelligence and statistics*. PMLR. 2021, pp. 343–351.
- 571 [69] B. Reddy, S. Tripathy, M. Vershinin, M. Tanenbaum, J. Xu, M. Mattson-Hoss, K. Arabi, D. Chapman, T. Doolin, C. Hyeon, and S. P.
572 Gross. "Heterogeneity in kinesin function". *Traffic* (2017).
- 573 [70] B. Reddy, N. Allipeta, and S. Gross. "A new method to experimentally quantify dynamics of protein-protein interactions" (2023). under
574 review.
- 575 [71] D. Gillespie. "Stochastic Simulation of Chemical Kinetics". *Annual Review of Physical Chemistry* (2007).
- 576 [72] P. Kloeden and P. E. "Numerical Solution of Stochastic Differential Equations". *Springer* (1992).

577 Supplementary Figures

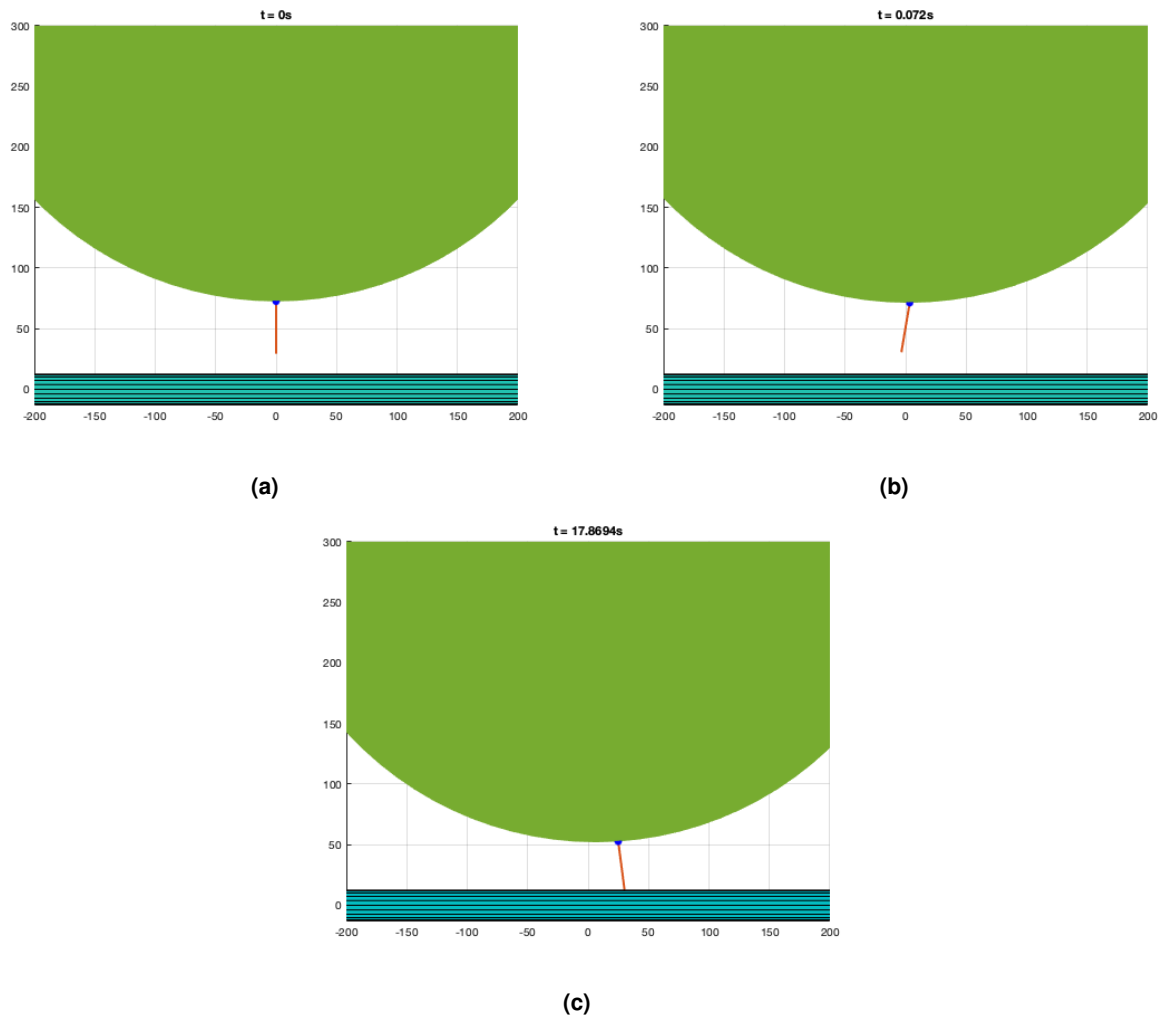


Figure S.1: Simulation Snapshots. The simulation starts as in **A**, where the motor (red line) is anchored (blue dot) to the bottom of the cargo (green sphere). The microtubule (turquoise cylinder) is centered at (0,0), and the axes depict locations of other components with respect to the microtubule center, in nanometers. As the simulation continues, the cargo and the motor diffuses with respect to force laws (b). The simulation ends when the motor strongly binds to the microtubule (c). Time (seconds) at which each event occurs is shown above figures.

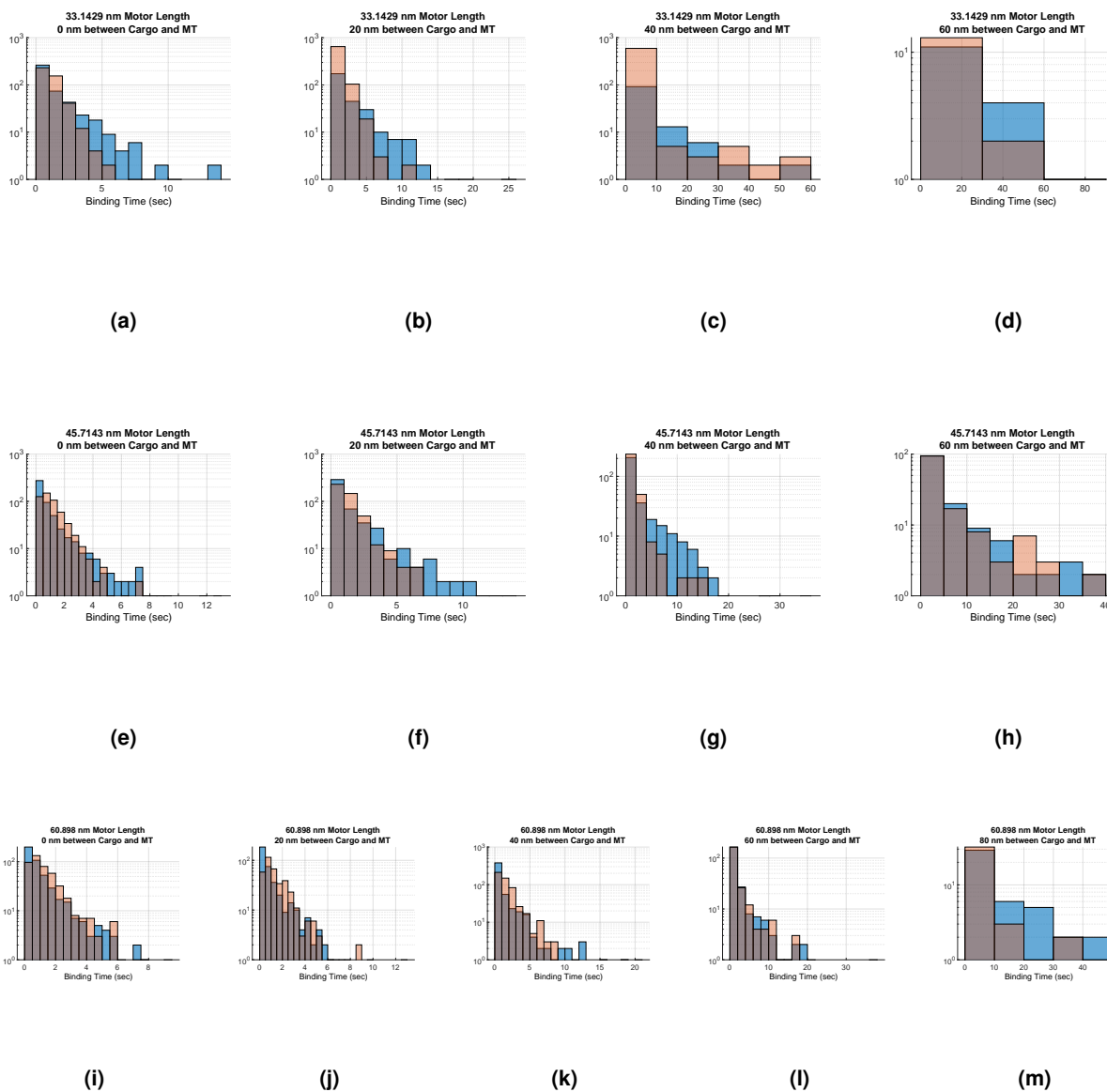


Figure S.2: Full distributions of binding times. Simulated data from ADP release model (red) is plotted over experimental data (blue). Overlap between distributions is shown in grey.

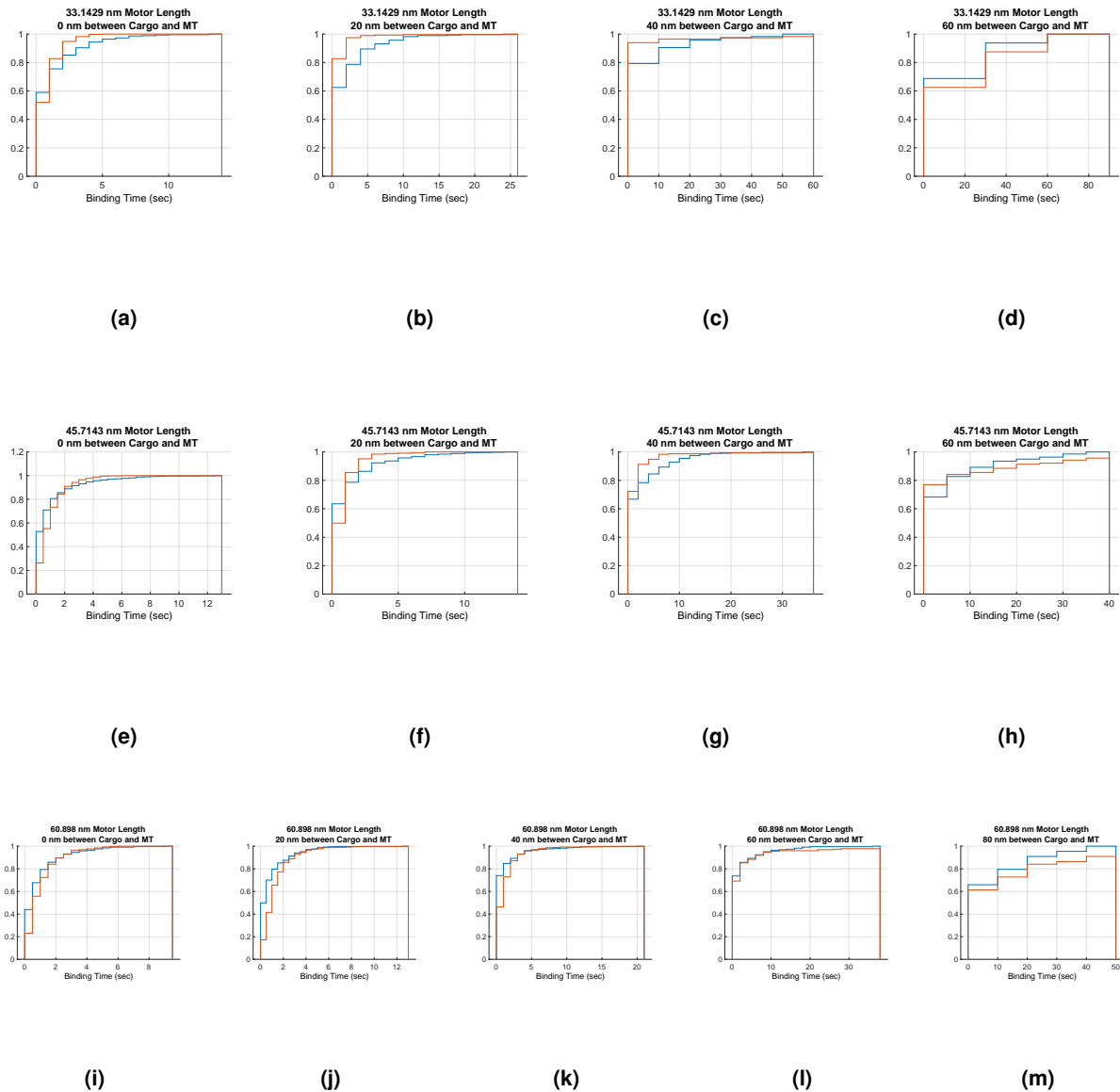


Figure S.3: Cumulative distributions of binding times. Simulated data from ADP release model (red) is plotted over experimental data (blue). Same information as Fig. S.2 but CDF instead of PDF.

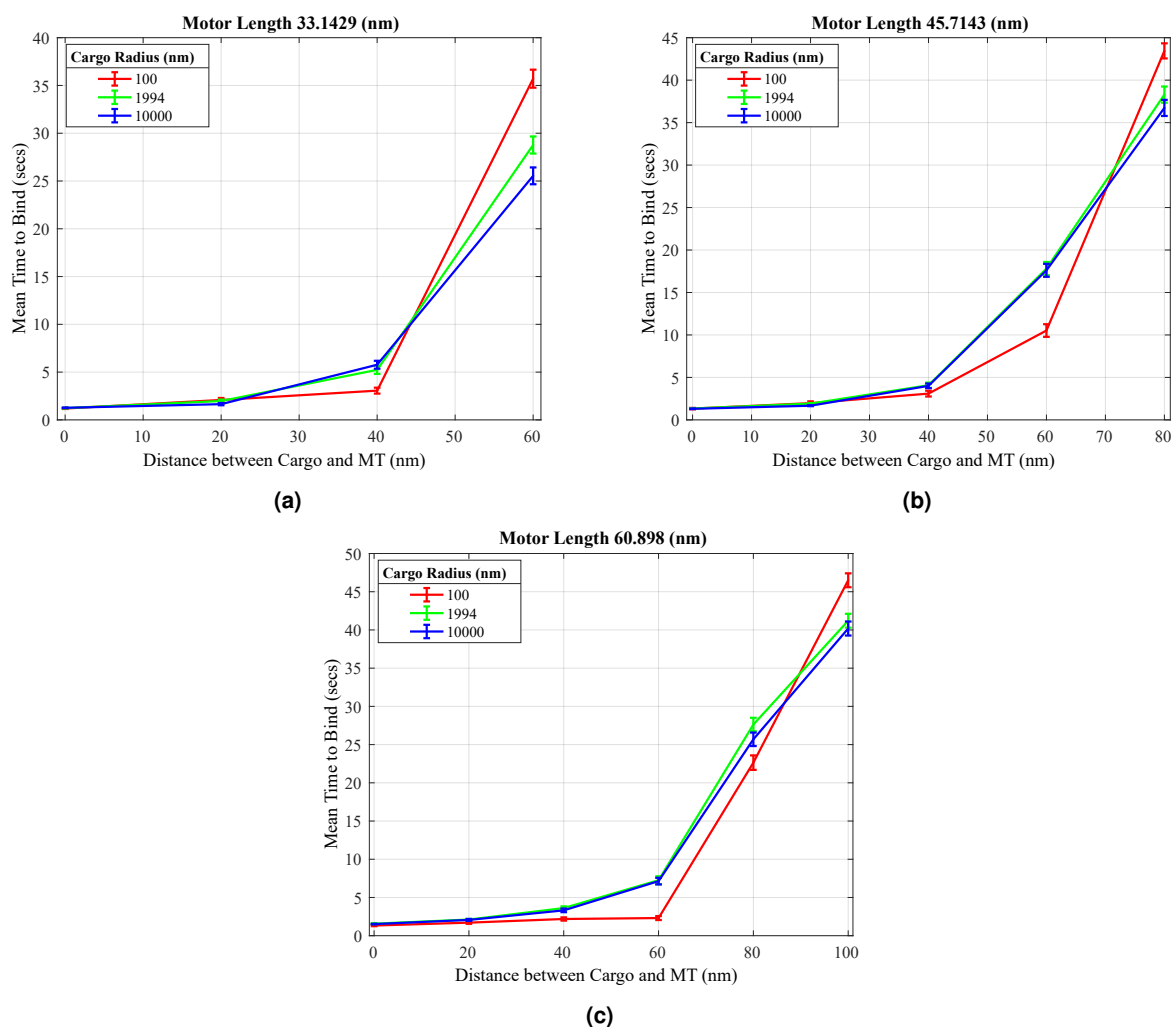


Figure S.4: Influence of motor head diffusion on binding time. A parameter sweep of the diffusion constant was conducted. Data are presented as mean \pm SEM.

Parameter	Simulated Value	Estimated Value
$k_{\text{off}}^{\text{ADP}}$	0.8	0.78
$k_{\text{on}}^{\text{ADP}}$	1000	1021.3
$k_{\text{off}}^{\text{ADP, Fast}}$	6.3	6.22
$k_{\text{on}}^{\text{MT}}$	10	9.83
$k_{\text{off}}^{\text{MT}}$	1	0.89
D_m	1000	987.56
κ_w	0.005	0.0057

Table S.1: Posterior Density Method Validation. Fake data was simulated using the ADP release model and the Simulated Values. A sequential Monte Carlo approximate Bayesian computational algorithm was performed on the fake data and recovered the simulated values (Estimated Value).

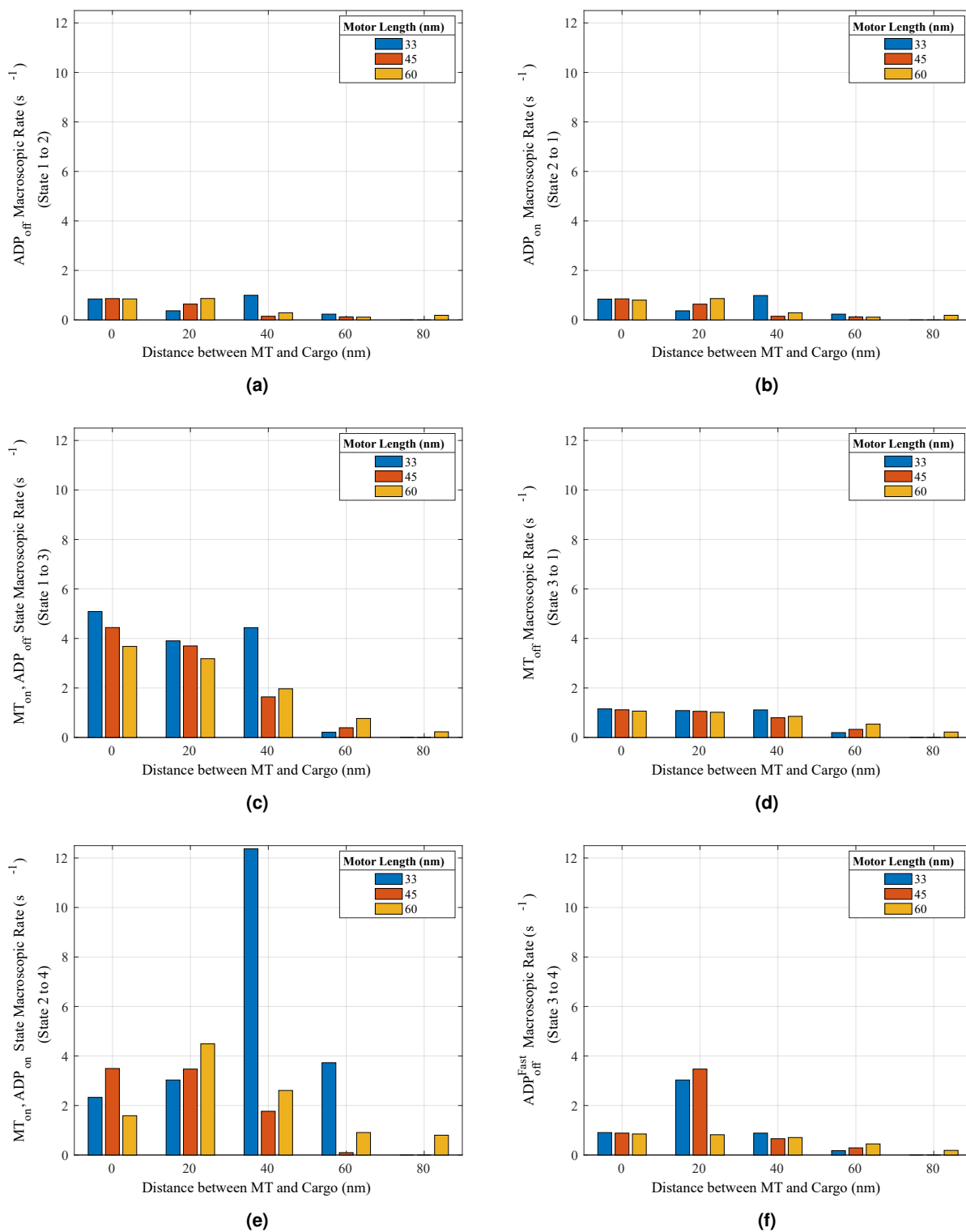


Figure S.5: Macroscopic rates of state transitions. Rates for each transition in the ADP+Diffusion model estimated with respect to average distance between the microtubule and the cargo for each motor length. Parameters from **Table 1** were used.

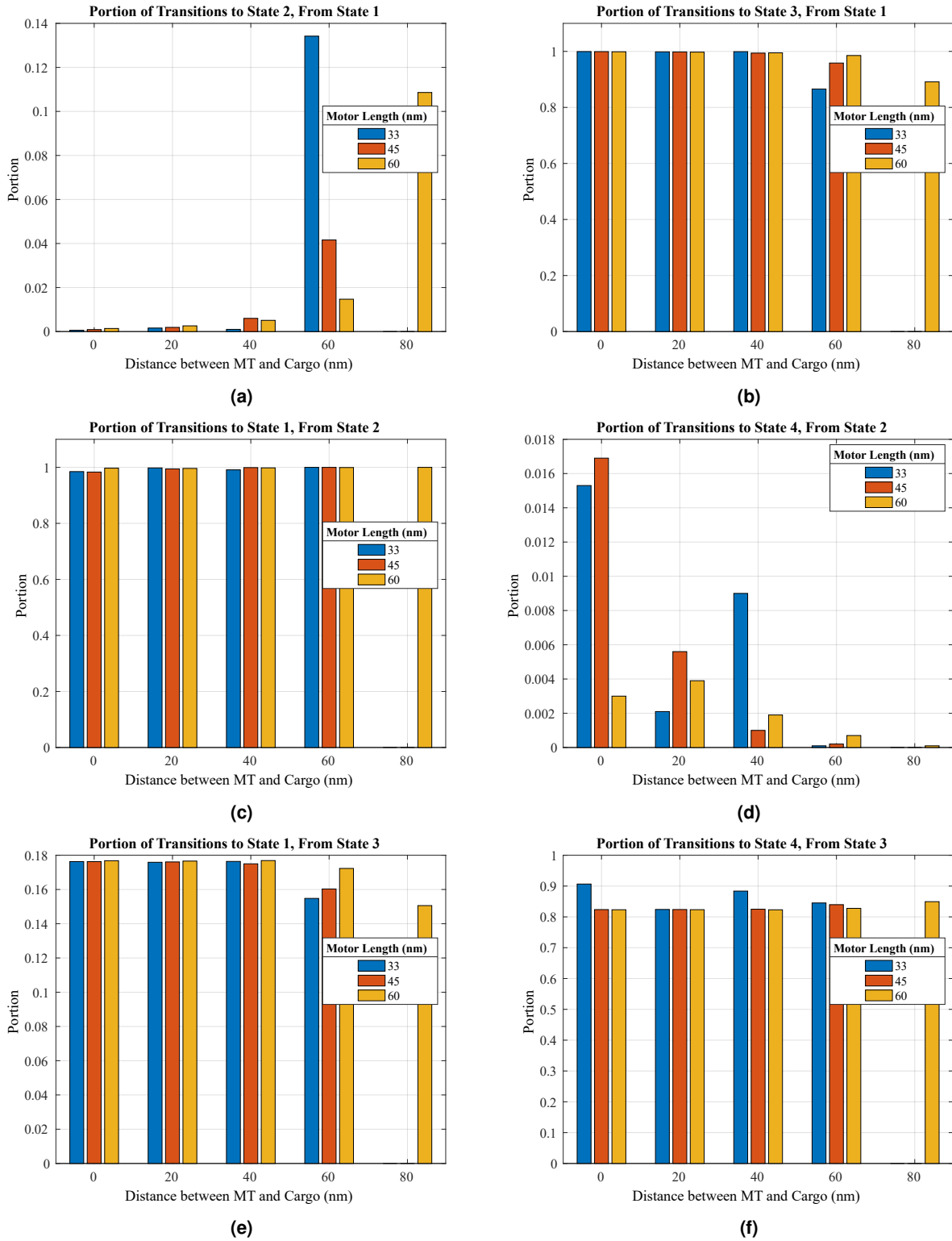


Figure S.6: Proportion of Transitions. Two transitions are possible for each state, and portion of each transition are graphed. Parameters from **Table 1** were used.

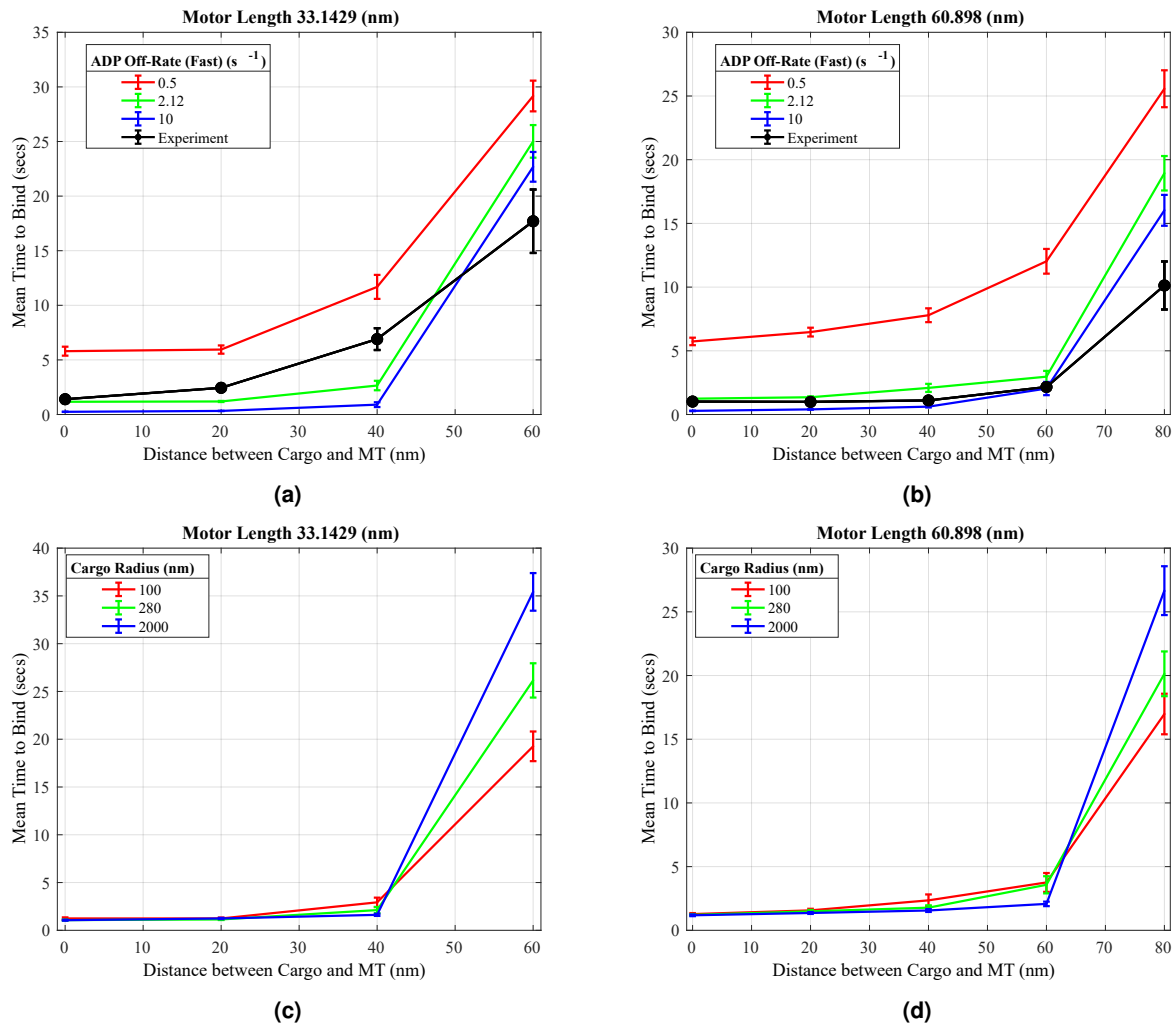


Figure S.7: Other Parameter Sweeps on Binding Times. $k_{off}^{ADP, Fast}$ (a-b) and cargo size (c-d) were varied in the ADP release model. Data are presented as mean \pm SEM.

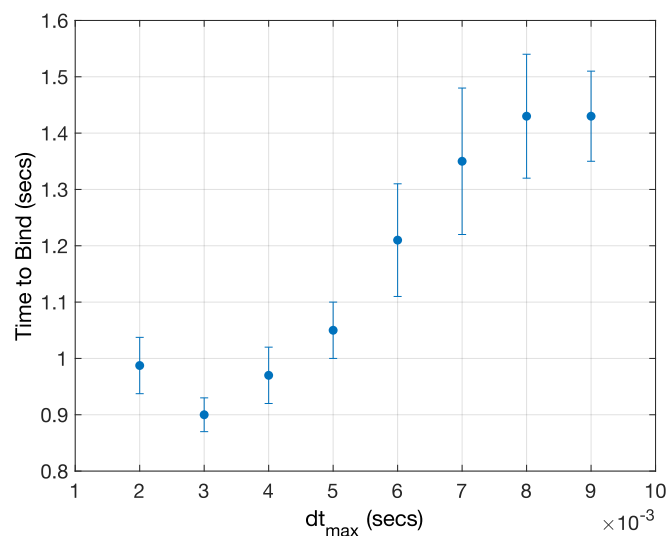
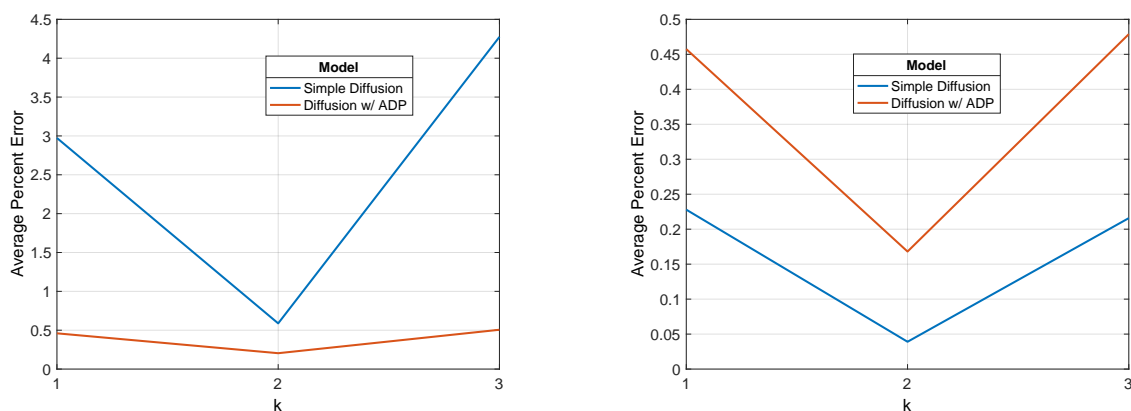


Figure S.8: Time step convergence study. Maximum time step was varied and converged to a common binding time. 0.004 was the largest maximum time step that resulted in a binding time that is relatively similar to the results from smaller maximum time step. $n = 1000$.



(a) Synthetic data from ADP release model

(b) Synthetic data from Simple Diffusion model

Figure S.9: Cross-Validation Test. Synthetic data was simulated using either the ADP release model **A** or the Simple Diffusion model **(b)**, and both the ADP release and the Simple Diffusion models' performance were evaluated using k -fold cross-validation.